Dietary Fiber Monosaccharide Content Alters Gut Microbiome Composition and Fermentation *In Vitro*

By

NICK M. JENSEN

THESIS

Submitted in partial satisfaction of the requirements for the degree of

MASTER OF SCIENCE

in

Microbiology

in the

OFFICE OF GRADUATE STUDIES

of the

UNIVERSITY OF CALIFORNIA

DAVIS

Approved:

David Mills, Chair

Diana Taft

Carlito Lebrilla

Committee in Charge

2022

ABSTRACT

Dietary Fiber Monosaccharide Content Alters Gut Microbiome Composition and Fermentation *In Vitro*

Members of the mammalian gut microbiota metabolize dietary carbohydrates that are not digested by the host. While the enzymes and transporters that each strain uses to establish a nutrient niche in the gut are often exquisitely specific, the relationship between carbohydrate structure and microbial ecology is imperfectly understood. The present study takes advantage of recent advances in complex carbohydrate structure determination to test the effects of fiber monosaccharide composition on microbial fermentation. Catabolism of human milk oligosaccharides (HMOs) by the genus *Bifidobacterium* is reviewed to illustrate gut microbial metabolism of specific dietary fiber structures and the resulting production of acidic microbial metabolites (AMMs), such as acetic acid. In the present study, 55 fibers with varied monosaccharide composition are fermented by a pooled feline fecal inoculum in a modified MiniBioReactor array (MBRA) system over a period of 72 hours. The content of the monosaccharides glucose and xylose and the concentration of the AMMs acetic acid, propionic acid, glyceric acid, and indole-3-acetic acid are significantly associated with the reduction of pH during fermentation. Microbiome diversity and composition are also significantly associated with monosaccharide content and AMM concentration, suggesting that monosaccharide composition offers a generalizable method to compare any dietary fiber of interest and uncover unexplored links between diet, the gut microbiota, and metabolite production.

ACKNOWLEDGEMENTS

I would like to thank everyone who worked in the Mills laboratory during my time there and to especially recognize the invaluable support and encouragement I received from Dr. David Mills, Dr. Diana Taft, and Dr. Karen Kalanetra. I appreciate our collaborators in the Lebrilla laboratory, whose expertise was vital to the success of this project. Thank you to all my professors for teaching me about the complex biology of bacteria and to my classmates in the Microbiology Graduate Group for their camaraderie (at least in the first two years before we retreated into our labs forever). Thank you to my mother for inspiring my sense of wonder about the natural world, my father for instilling my love of reading and disorganized curiosity, and my sister for judging me when I'm tempted to become a lotus-eater. Thank you to Carl Basbas and his family for making me feel welcome during my time in California and tolerating my cow jokes. Thank you to my own gut bacteria for helping metabolize my favorite vegetables. Finally, thank you to Per Petterson and various Instagram influencers for teaching me that "we do decide for ourselves when it will hurt."

Chapter 1

How nursing mothers protect their babies with bifidobacteria

Nick Jensen[1,2], Britta E. Heiss[1,2] and David A. Mills[1,2]

[1]Department of Food Science and Technology, [2]Foods for Health Institute, University of California Davis, One Shields Avenue, Davis, CA 95616, USA.

Published in Jensen NM, Heiss BE, Mills DA. 2022. How nursing mothers protect their babies with bifidobacteria, p. 13–21. *In* de Bruijn, FJ, Smidt, H, Cocolin, L, Sauer, M, Dowling, DN, Thomashow, L (eds.), The Good Microbes in Medicine, Food Production, Biotechnology, Bioremediation, and Agriculture. John Wiley & Sons Ltd.

Abstract

Bifidobacterium species are common residents of the human gastrointestinal tract. While they colonize people of all ages, they are most strikingly found in the infant gut, where they degrade human milk oligosaccharides (HMOs) found in breast milk. Individual *Bifidobacterium* strains encode unique sets of transport proteins and enzymes called glycoside hydrolases (GHs) to metabolize these diverse carbohydrates in milk. By fermenting HMOs, bifidobacteria produce bioactive end products such as lactate and acetate. These molecules reduce the pH of the gut and protect against invasion by harmful pathogens and likely support healthy childhood growth and immune development. Although *Bifidobacterium* colonization promotes infant health, levels of these bacteria vary based on geography, breastfeeding rates and other factors. However, recent trials suggest that providing infants with probiotic *Bifidobacterium*, in combination with HMOs that sustain their nutrient niche, can support the persistent growth of these beneficial bacteria.

1.1. *Bifidobacterium* Species and Diversity

Just as humans require air, water, food and a place to live, microbes require a stable, moist habitat with an abundant store of energy. But for some bacteria, air can be deadly. Unlike most multicellular organisms, many microbes will die in the presence of oxygen, leading them to seek out environments that are reliably anaerobic. For many of these bacteria, animal guts offer not only a respite from dangerous oxygen, but also a reliable source of food in the form of undigested carbohydrates like dietary fiber that pass through the digestive tract [12].

Bifidobacterium is one such genus of carbohydrate-degrading, oxygen-sensitive microbes. In the human gut, the majority of bacteria belong to the two large phyla Bacteroidetes and Firmicutes, with a few exceptions like the mucus-consuming *Akkermansia* [22]. *Bifidobacterium* is the main representative from an entirely different phylum called Actinobacteria, which also includes the soil-dwelling *Streptomyces* that produces many medically-important antibiotics [4]. Like their environmental relatives, bifidobacteria excel at metabolizing carbohydrates, but they are too sensitive to oxygen to make a living on the forest floor. Despite this handicap, bifidobacteria can live inside a remarkable range of hosts. While many bacteria exhibit restricted associations, bifidobacteria have been isolated from animals as diverse as bees, chickens, cattle, lemurs and humans [36]. From humans alone, at least nine species have been discovered [8].

However, these species are not evenly distributed among all humans. Indeed, their ability to colonize humans appears strikingly age dependent. The genus *Bifidobacterium* was originally discovered because of its specific association with babies. In 1899, Henri Tissier identified the first known *Bifidobacterium* when he discovered that the feces of a breastfed infant was dominated by distinctive Y-shaped bacteria [51]. We now know that some *Bifidobacterium* species are found almost exclusively in babies and toddlers, such *as B. breve*. Other species, like *B. catenulatum* and *B. adolescentis*, generally do not appear until after weaning. Some

species are more cosmopolitan. *B. bifidum* and *B. longum*, for example, inhabit people of all ages [28]. However, when considering all *Bifidobacterium* strains, their relative abundance appears to decline with the age of the human host [28].

1.2 Human Milk Oligosaccharides

While multiple factors may underlie age-dependent changes in *Bifidobacterium* levels, diet is likely the primary reason that bifidobacteria tend to be more common in infants. Bifidobacteria lack the enzymes needed to attack the large, intact fiber molecules that many other gut microbes can process. After these other bacteria, such as *Bacteroides*, break up complex fiber molecules into simpler carbohydrates called oligosaccharides, bifidobacteria latch onto these substrates as a more accessible energy source [11]. Since most of undigested carbohydrates in our diet are bulky fibers, bifidobacteria generally rely on pre-degraded byproducts of other microbes to obtain their nutrition.

But there is one food in the human diet whose carbohydrates are already the perfect size for bifidobacteria: breast milk. After lactose and lipids, the third-largest component of breast milk is a wide array of human milk oligosaccharides (HMOs) [33]. Although other mammals also produce milk oligosaccharides, human milk contains the most diverse, complex and abundant oligosaccharides of any species [53]. Their structures are elaborately decorated with rare monomeric sugars like sialic acid and fucose that are found in few plant foods [6]. Yet the enzymes required to digest them are not expressed in humans—adults or infants. On their own, HMOs may provide babies with some benefits, such as strengthening the integrity of the intestinal barrier [10]. But most of them pass untouched through the gut, where infant-specialized bifidobacteria like *Bifidobacterium longum* subsp. *infantis* and *B. breve* readily metabolize them. When HMOs are provided, infant-associated *Bifidobacterium* gain a metabolic advantage, and few other gut bacteria can outcompete them for the nutrient resource [15].

While they primarily consume free HMOs, infant-associated bifidobacteria may also metabolize other components of milk, such as milk glycans (the carbohydrate components of glycoproteins) [23, 29].

1.3. Bifidobacterial Metabolism

In order to metabolize HMOs, bifidobacteria rely on specialized classes of genes. *Bifidobacterium* species possess numerous genes encoding enzymes called glycoside hydrolases (GHs), which are necessary for metabolizing complex carbohydrates, as well as transport systems that import GH breakdown products [15]. Most bifidobacteria import oligosaccharides directly into the cell and metabolize the entire molecule, although some may only break off pieces and leave leftover HMO portions for other microbes to consume (Fig. 1.1) [43]. Either way, all *Bifidobacterium* species encode a wide repertoire of GHs and transporters that allow them to target specific oligosaccharides. *Bifidobacterium* strains exhibit significant heterogeneity in their GH content, with closely related strains often metabolizing distinct substrates. Most *B. longum* subsp. *longum* strains express a range of GHs that degrade plant-derived oligosaccharides; however, some strains encode a gene cluster that allows them to consume fucosylated HMOs [20].

These metabolic differences afford each species and strain a degree of specialization that allows it to establish its own ecological niche in the intestine. Since HMOs are so diverse, many bifidobacteria preferentially consume certain subtypes, like fucosylated HMOs. Only one subspecies, *B. longum* subsp. *infantis*, has enough GHs and transporters to metabolize all known HMOs [42]. Some of these transporters may import multiple HMOs, while others assimilate a restricted set, though many remain uncharacterized [41]. Transporters are often encoded in clusters with substrate-binding proteins (SBPs) that allow individual strains to sequester particular HMOs [19]. Operating in concert, these proteins equip each

Bifidobacterium strain with unique metabolic capabilities that explain the wide range of growth phenotypes observed among related strains [7, 37].

These diverse growth phenotypes, whereby some strains preferentially consume a selective portion of the HMO pool while others degrade portions of that pool externally, leaving simple sugars behind, may foster resource sharing communities of *Bifidobacterium* strains. In fact, multiple *Bifidobacterium* species routinely co-occur in the microbiome of a single infant [56]. The specific composition of *Bifidobacterium* strains may vary widely between individuals in both infants and adults, suggesting that there is no single phenotype that consistently outperforms competitors over the entire human lifespan and range of diets [52, 55]. Instead, local conditions, such as HMO composition [45], host genetics [31] and background microbiota [54], may lead to a unique partitioning of resources between colonizing strains.

1.4. Benefits of *Bifidobacterium*

As bifidobacteria thrive on the HMOs in breast milk, their growth also offers several benefits for their infant hosts. Bifidobacteria convert HMOs into metabolites that help babies grow and avoid illness. When bifidobacteria metabolize HMOs, they ferment them into bioactive end products. Using the enzyme fructose-6-phosphate phosphoketolase in a specialized pathway called the “bifid shunt,” *Bifidobacterium* strains produce a characteristic 3:2 molar ratio of acetate to lactate [42]. Both of these molecules are acidic, so they lower the pH of the gut. In a cohort of Bangladeshi children, an elevated fecal pH was linked to increased levels of childhood stunting, suggesting that the lactate and acetate may be protective [26]. Another study of Bangladeshi children recovering from malnutrition suggested that certain gut microbes, including *Bifidobacterium*, were associated with proteins that regulate childhood growth [21]. Acetate is a short-chain fatty acid, a major class of microbial metabolites that has been intensely studied for its benefits to humans [5, 38]. In mice, acetate produced by the microbiota can protect against

infection by respiratory syncytial virus, a major cause of infant mortality, by signaling through the host receptor Gpr43 [2]. A similar mechanism may operate in human infants.

Bifidobacterium that ferment HMOs may also offer indirect benefits by preventing infection by pathogenic bacteria. Protection from harmful invaders, a phenomenon termed colonization resistance to pathogens, is another important service provided by gut microbes like *Bifidobacterium* [39]. Low pH provides an obstacle to infection by dangerous bacteria like the foodborne pathogen *E. coli* O157:H7. In mice, acetate produced by *Bifidobacterium* limits the dissemination of Shiga toxin by strengthening the intestinal barrier [18]. During the first month of life, fecal samples from cohort of Japanese infants colonized by *Bifidobacterium* had lower pH and higher acetate concentrations [35]. In addition, *Bifidobacterium* levels were negatively correlated with the relative abundance of Enterobacteriaceae, a family of bacteria that includes most common human pathogens. In breastfed infants supplemented with *B. longum* subsp. *infantis*, fecal levels of proinflammatory cytokines were associated with Enterobacteriaceae and negatively correlated with *Bifidobacterium* relative abundance [24]. Recently, Casaburi et al. reported that a single strain of *Bifidobacterium longum* subsp. *infantis* provided to breastfed infants could reduce levels of fecal inflammatory markers and virulent endotoxin-producing bacteria and possibly protect intestinal barrier integrity by limiting mucus breakdown [9].

Blocking Enterobacteriaceae may also reduce the level of antibiotic resistance genes in the gut. When the gut microbiome of Bangladeshi infants was dominated by *Bifidobacterium*, it was found to contain fewer total antibiotic resistance genes and fewer classes of antibiotic resistance gene. This protective effect appeared to last until age 2, possibly because the infants were colonized by a more diverse microbiota during weaning [50]. *Bifidobacterium* may also assist in immune system development by boosting vaccine responses. At age 2, mean *Bifidobacterium* abundance was associated with improved CD4+ T cell responses to essential vaccines against tetanus and hepatitis B [27].

1.5. Global Distribution of *Bifidobacterium*

Given the many positive health outcomes associated with early, and predominant, colonization of infants by *Bifidobacterium*, supporting these microbes could benefit public health. However, fecal metagenome samples from around the world suggest that, during the first 6 months of life, even exclusively breastfed infants vary in *Bifidobacterium* species composition and prevalence, with some regions exhibiting high levels of *Bifidobacterium* colonization (often with >50% relative abundance) [3, 27, 30, 50, 59]; and others exhibiting a lower abundance (0-30%) [16, 31, 60]. For example, *Bifidobacterium* relative abundance appears higher in Russia than Finland and Estonia [60], and higher in Indonesia than New Zealand [30].

Many variables may drive this variation in *Bifidobacterium* levels, including population-level breastfeeding rates, sanitation and hygiene practices, antibiotic usage, and birth delivery mode. Such factors may diminish *Bifidobacterium* levels or deplete specific HMO-catabolizing strains in the environment of the mother-infant dyad, thereby altering the level and time course of *Bifidobacterium* colonization in early life. Vatanen et al. found that infants were dominated by either *B. longum*, *B. bifidum* or *B. breve*, with *B. longum* containing HMO-utilization genes being more common in breastfed infants [59]. In a cohort of Swedish infants, *Bifidobacterium* was common in infants at 4 months of age, but only in breastfed infants was it still dominant at 12 months [3]. Metagenomic samples from an Italian cohort suggested that individual *Bifidobacterium* strains may be transferred from mother to infant, so factors that affect a mother's gut, skin and vaginal microbiota may indirectly impact the colonization of her baby [16]. These studies reveal that the contemporary picture of the *Bifidobacterium*-infant association is far more complex than initial reports suggested. While it is not completely certain that *Bifidobacterium* levels have changed over time since their discovery in 1899, the average pH of infant feces has increased from 5.0 to 6.5 between 1926 and 2017 [25]. Such a dramatic

increase in pH suggests that the composition of the infant microbiome has shifted over a relatively short time, possibly because of inconsistent breastfeeding rates.

1.6. Supporting Persistent *Bifidobacterium* Populations

Since *Bifidobacterium* do not predominate in the microbiota of all infant cohorts, researchers hope to determine how to successfully seed and support the growth of these beneficial bacteria. Strains within the genus *Bifidobacterium* are often administered as probiotics for newborns and infants. Probiotics containing *Bifidobacterium* may help prevent or treat necrotizing enterocolitis, infantile colitis, acute diarrhea, obesity, allergies, and celiac disease [13]. Despite strong health associations, the mechanism of action for such probiotics is poorly understood, although it may involve known pathways such as acetate production. Regardless, these benefits depend on establishing persistent populations of *Bifidobacterium* within the host gut.

Breast milk may provide a nutrient niche that allows *Bifidobacterium* strains to persist if they have the appropriate metabolic genes. In a trial comparing two *Bifidobacterium* strains as probiotics for preterm infants, only *Bifidobacterium longum* subsp. *infantis* persisted in infants fed human milk. *Bifidobacterium animalis* subsp. *lactis*, which lacks the genes to metabolize HMOs, was unable to compete even when it was given as a supplement [57]. Recently, Frese et al. showed dramatic and persistent colonization of an HMO-catabolizing strain of *Bifidobacterium longum* subsp. *infantis* that was given as a supplement to breastfed infants [17]. In infants with persistent *B. longum* subsp. *infantis*, fecal acetate and lactate were elevated, while pH was reduced. These infant cohorts demonstrate that the provision of an HMO-catabolizing *Bifidobacterium* can support stable engraftment across an infant population.

Bifidobacterium may be more likely to persist than other beneficial bacteria when HMOs are provided. Like *Bifidobacterium*, *Lactobacillus* species are often administered, both alone and in consortia, in infant probiotics designed to reduce necrotizing enterocolitis and infantile colic [32, 49]. In preterm infants supplemented with *Lactobacillus* as well as *Bifidobacterium*, only *Bifidobacterium* robustly persisted. Furthermore, *Bifidobacterium* levels correlated with the metabolism of HMOs, as measured by the production of fecal acetate. While *Lactobacillus* persistence was merely transient, the supplemented *Bifidobacterium* either persisted itself or improved the persistence of other *Bifidobacterium* species [1]. Clearly, the two microbes were not equivalent for this probiotic application.

Research on other microbes may explain the discrepancy by demonstrating the fundamental importance of a "metabolic niche." In both mice and humans recovering from antibiotics, a mixed-species probiotic failed to persist and also delayed the reconstitution of the microbiota compared to a fecal microbial transplant derived from a pre-antibiotic sample [48]. Press coverage of this study prompted a wave of articles questioning the overall efficacy of probiotics. However, the *Lactobacillus* and *Bifidobacterium* species in this study's probiotic were not administered along with an appropriate carbohydrate source. "Microbiota-accessible carbohydrates" are critical for supporting populations of gut bacteria, and declining rates of dietary fiber consumption may cause the extinction of microbes bereft of a carbon source [46–47]. Conversely, providing a unique metabolic niche can permit a single strain of a gut bacterium like *Bacteroides* to outcompete related microbes that lack the enzymatic machinery needed to degrade a target carbohydrate [44]. *Bifidobacterium* species, not *Lactobacillus*, generally encode the enzymes and transporters needed to degrade the HMOs in the infant diet, explaining why they were able to persist. Probiotics may prove more effective if they are supported by an appropriate dietary modification.

The metabolic niche established by HMO-consuming *Bifidobacterium* species may also depend on transport proteins. Just as a unique enzyme can allow a microbe to access a new

carbohydrate, strains possessing specific transporters may enjoy a competitive advantage and more effectively colonize the human gut [34]. Similarly, an analysis of infant metagenomes revealed that HMO-specific transporters influence *Bifidobacterium* ability to colonize the infant gut. Sakanaka et al. found that the abundance of an HMO-specific transporter was correlated with *Bifidobacterium* relative abundance [41]. However, such an association may be geographically-dependent. When examining infant cohorts by country, a strong correlation between transporters and *Bifidobacterium* levels was detected for Malawian and Venezuelan infants, but not infants in the United States.

Fitness differences in the infant gut may also be explained by distinct mechanisms of HMO catabolism among *Bifidobacterium* species. Species such as *B. bifidum* often employ extracellular glycoside hydrolases instead of importing HMOs via transporters [40]. While these bifidobacteria are generally present in surveys of infant microbial communities, species that more commonly take in HMOs via transporters (such as *B. pseudocatenulatum* and *B. longum* subsp. *infantis*) are often detected at a higher relative abundance [31, 35].

Such mechanistic differences underscore the importance of studying individual *Bifidobacterium* strains. While *Bifidobacterium* species and subspecies are traditionally characterized based on generalized estimates of metabolic capabilities, recognizing strain-specific differences in HMO catabolism is critical for selecting appropriate species to promote beneficial outcomes in the infant gut. A comparison of *Bifidobacterium* HMO utilization genes suggested that 14 *B. longum* subsp. *infantis* isolates could be classified into three distinct genomic variants. *B. longum* subsp. *infantis* genetically lacking an ABC-type transporter displayed a growth disadvantage in competitive assays against a strain possessing the transporter when grown on an isolated HMO. While these data were obtained *in vitro,* they indicate that genotypic variation can underlie differences HMO growth ability [14].

These genotypic differences can result in fitness differences in the infant gut environment. In a retrospective cohort study of preterm, breastfed infants provided a probiotic

containing *B. infantis* and *L. acidophilus*, 75% of the infants still maintained a population of *B. longum* subsp. *infantis* four weeks after probiotic cessation. However, after a second round of probiotic administration, *Bifidobacterium longum* subsp. *longum* failed to persist, likely due to its competitive disadvantage in metabolizing HMOs [58]. While we cannot be certain that the probiotic *B. longum* subsp. *infantis* was identical to the detected strain, as transient populations of *Bifidobacterium* circulate in NICUs (neonatal intensive care units), these data suggest that *Bifidobacterium* differ at the strain level in their ability to persist in the infant gut. Underwood et al. obtained similar results by administering HMO-catabolizing *B. longum* subsp. *infantis* non-HMO-catabolizing *B. animalis* subsp. *lactis* in a crossover trial of breastfed infants [57]. Regardless of the probiotic administered, HMO-catabolizing *Bifidobacterium* were the most highly represented within the infant microbiome, demonstrating that they enjoy an advantage in infant colonization due to HMO catabolism.

1.7. Summary

Many health benefits are clearly linked to the common colonization of the breastfed infant gut by *Bifidobacterium* species. *Bifidobacterium* species produce lactate and acetate that may exclude pathogenic bacteria and support growth and immune development. These protective molecules are produced by fermenting complex human milk oligosaccharides, which support a specialized ecology of *Bifidobacterium* species. This natural enrichment demonstrates that appropriate dietary carbohydrates can nourish specific, and beneficial, gut microbial niches. Further research on the mechanisms underlying this enrichment will drive novel dietary and probiotic interventions that enable persistence of beneficial *Bifidobacterium* strains in vulnerable populations of any stage of life.

Acknowledgements

This study was supported by National Institutes of Health awards 5T32AI060555 (BEH), RO1AT008759 (DAM) and the Peter J. Shields Endowed Chair in Dairy Foods (DAM). Figure 1.1 was created, in part, with BioRender.com

REFERENCES

1. Alcon-Giner C, Dalby MJ, Caim S, Ketskemety J, Shaw A, et al. 2020. Microbiota supplementation with *Bifidobacterium* and *Lactobacillus* modifies the preterm infant gut microbiota and metabolome: an observational study. *Cell Reports Medicine*. 1:100077.
2. Antunes KH, Luís Fachi J, de Paula R, Fraga da Silva E, Passariello Pral L, et al. 2019. Microbiota-derived acetate protects against respiratory syncytial virus infection through a GPR43-type 1 interferon response. *Nature Communications*. 10:1-17.
3. Bäckhed F, Roswall J, Peng Y, Feng Q, Jia H, et al. 2015. Dynamics and stabilization of the human gut microbiome during the first year of life. *Cell Host & Microbe*. 17:690-703.
4. Biavati B, Mattarelli P. 2018. Related genera within the family Bifidobacteriaceae, p 49-66. *In* Mattarelli P, Biavati B, Holzaphel WH, Wood BJB (eds), *The Bifidobacteria and Related Organisms*, Academic Press - Elsevier, London UK.
5. Blaak EE, Canfora EE, Theis S, Frost G, Goren AK, et al. 2020. Short chain fatty acids in human gut and metabolic health. *Beneficial Microbes*. 11:411-455.
6. Bode L, Jantscher-Krenn E. 2012. The glycobiology of human milk oligosaccharides structure-function relationships of human milk oligosaccharides. *Advances in Nutrition*. 3:383-391.
7. Bottacini F, O'Connell Motherway MO, Kuczynski J, O'Connell KJ, Serafini F, et al. 2014. Comparative genomics of the *Bifidobacterium breve* taxon. *BMC Genomics*. 15:170.
8. Bottacini F, Ventura M, van Sinderen D, Motherway MOC. 2014. Diversity, ecology and intestinal function of bifidobacteria. *Microbial Cell Factories*. 13: S4.
9. Casaburi G, Karav S, Frese S, Henrick B. 2019. Gut barrier function is improved in infants colonized by *Bifidobacterium longum* subsp. *infantis* EVC001 (FS04-05-19). *Current Developments in Nutrition*. 3(Supplement_1):932.
10. Chichlowski M, De Lartigue G, German JB, Raybould HE, Mills DA. 2012. Bifidobacteria isolated from infants and cultured on human milk oligosaccharides affect intestinal epithelial function. *Journal of Pediatric Gastroenterology and Nutrition*. 55:321-327.
11. Cockburn DW, Koropatkin NM. 2016. Polysaccharide degradation by the intestinal microbiota and its influence on human health and disease. *Journal of Molecular Biology*. 428:3230-3252.
12. Deehan EC, Walter J. 2016. The fiber gap and the disappearing gut microbiome: Implications for human nutrition. *Trends in Endocrinology & Metabolism*. 27:239-242.
13. Di Gioia D, Aloisio I, Mazzola G, Biavati B. 2014. Bifidobacteria: their impact on gut microbiota composition and their applications as probiotics in infants. *Applied Microbiology and Biotechnology*. 98:563-577.

14. Duar RM, Casaburi G, Mitchell RD, Scofield LNC, Ortega Ramírez CA, et al. 2020. Comparative genome analysis of *Bifidobacterium longum* subsp. *infantis* strains reveals variation in human milk oligosaccharide utilization genes among commercial probiotics. *Nutrients*. 12:3247.
15. Egan M, van Sinderen D. 2018. Carbohydrate metabolism in bifidobacteria, p 145-164. *In* Mattarelli P, Biavati B, Holzaphel WH, Wood BJB (eds), *The Bifidobacteria and Related Organisms*, Academic Press - Elsevier, London UK.
16. Ferretti P, Pasolli E, Tett A, Ascinar F, Gorfer V, et al. 2018. Mother-to-infant microbial transmission from different body sites shapes the developing infant gut microbiome. *Cell Host & Microbe*. 24:133-145.
17. Frese SA, Hutton AA, Contreras LN, Shaw CA, Palumbo MC, et al. 2017. Persistence of supplemented *Bifidobacterium longum* subsp. *infantis* EVC001 in breastfed infants. *mSphere*. 2:e00501-17.
18. Fukuda S, Toh H, Hase K, Oshima K, Nakanishi Y, Yoshimura K, et al. 2011. Bifidobacteria can protect from enteropathogenic infection through production of acetate. *Nature*. 469:543-547.
19. Garrido D, Kim JH, German JB, Raybould HE, Mills DA, et al. 2011. Oligosaccharide binding proteins from *Bifidobacterium longum* subsp. *infantis* reveal a preference for host glycans. *PLoS One*. 6:e17315.
20. Garrido D, Ruíz-Moyano S, Kirmiz N, Davis JC, Totten SM, et al. 2016. A novel gene cluster allows preferential utilization of fucosylated milk oligosaccharides in *Bifidobacterium longum* subsp. *longum* SC596. *Scientific Reports*. 6:35045.
21. Gehrig JL, Venkatesh S, Chang H-W, Hibberd MC, Kung VL, et al. 2019. Effects of microbiota-directed foods in gnotobiotic animals and undernourished children. *Science*. 365:eaau4732.
22. Gilbert JA, Blaser MJ, Gregory Caporaso J, Jansson JK, Lynch SV, et al. 2018. Current understanding of the human microbiome. *Nature Medicine*. 24:392-400.
23. González-Morelo KJ, Vega-Sagardía M, Garrido D. 2020. Molecular insights into O-linked glycan utilization by gut microbes. *Frontiers in Microbiology*. 11:591568.
24. Henrick BM, Chew S, Casaburi G, Brown HK, Frese SA, et al. 2019. Colonization by *B. infantis* EVC001 modulates enteric inflammation in exclusively breastfed infants. *Pediatric Research*. 86:749-757.
25. Henrick BM, Hutton AA, Palumbo MC, Casaburi G, Mitchell RD, et al. 2018. Elevated fecal pH indicates a profound change in the breastfed infant gut microbiome due to reduction of *Bifidobacterium* over the past century. *mSphere*. 3:e00041-18.
26. Hossain MS, Das S, Gazi MA, Alam MA, Haque NMS, et al. 2019. Association of faecal pH with childhood stunting: results from a cross-sectional study. *BMJ Paediatrics Open*. 3:1-6.

27. Huda MN, Ahmad SM, Alam MJ, Khanam A, Kalanetra KM, et al. 2019. *Bifidobacterium* abundance in early infancy and vaccine response at 2 years of age. *Pediatrics*. 143:e20181489.
28. Kato K, Odamaki T, Mitsuyama E, Sugahara H, Xiao JZ, et al. 2017. Age-related Changes in the Composition of Gut *Bifidobacterium* Species. *Current Microbiology*. 74:987-995.
29. Kirmiz N, Robinson RC, Shah IM, Barile D, Mills DA. 2018. Milk glycans and their interaction with the infant gut microbiota. *Annual Reviews in Food Science and Technology*. 9:429-450.
30. Lawley B, Otal A, Moloney-Geany K, Diana A, Houghton L, et al. 2019. Fecal microbiotas of Indonesian and New Zealand children differ in complexity and bifidobacterial taxa during the first year of life. *Applied and Environmental Microbiology*. 85:1-14.
31. Lewis ZT, Totten SM, Smilowitz JT, Popovic M, Parker E, et al. 2015. Maternal fucosyltransferase 2 status affects the gut bifidobacterial communities of breastfed infants. *Microbiome*. 3:13.
32. Liu D, Shao L, Zhang Y, Kang W. 2020. Safety and efficacy of *Lactobacillus* for preventing necrotizing enterocolitis in preterm infants. *International Journal of Surgery*. 76:79-87.
33. LoCascio RG, Ninonuevo MR, Freeman SL, Sela DA, Grimm R, et al. 2007. Glycoprofiling of bifidobacterial consumption of human milk oligosaccharides demonstrates strain specific, preferential consumption of small chain glycans secreted in early human lactation. *Journal of Agricultural and Food Chemistry*. 55:8914-8919.
34. Maldonado-Gómez MX, Martínez I, Bottacini F, O'Callaghan A, Ventura M, et al. 2016. Stable engraftment of *Bifidobacterium longum* AH1206 in the human gut depends on individualized features of the resident microbiome. *Cell Host & Microbe*. 20:515–526.
35. Matsuki T, Yahagi K, Mori H, Matsumoto H, Hara T, et al. 2016. A key genetic factor for fucosyllactose utilization affects infant gut microbiota development. *Nature Communications*. 7:11939.
36. Mattarelli P, Biavati B. 2018. Species in the genus *Bifidobacterium*, p 9-48. *In* Mattarelli P, Biavati B, Holzaphel WH, Wood BJB (eds), *The Bifidobacteria and Related Organisms*, Academic Press - Elsevier, London UK
37. Milani C, Turroni F, Duranti S, Lugli GA, Mancabelli L, et al. 2016. Genomics of the genus *Bifidobacterium* reveals species-specific adaptation to the glycan-rich gut environment. *Applied and Environmental Microbiology*. 82:980-991.
38. Postler TS, Ghosh S. 2017. Understanding the holobiont: how microbial metabolites affect human health and shape the immune system. *Cell Metabolism*. 26:110-130.
39. Romond MB, Haddou Z, Mielcareck C, Romond C. 1997. Bifidobacteria and human health: regulatory effect of indigenous bifidobacteria on *Escherichia coli* intestinal colonization. *Anaerobe*. 3:131-136.

40. Sakanaka M, Gotoh A, Yoshida K, Odamaki T, Koghuchi H, et al. 2020. Varied pathways of infant gut-associated *Bifidobacterium* to assimilate human milk oligosaccharides: Prevalence of the gene set and its correlation with bifidobacteria-rich microbiota formation. *Nutrients*. 12:1-21.
41. Sakanaka M, Hansen ME, Gotoh A, Katoh T, Yoshida K, et al. 2019. Evolutionary adaptation in fucosyllactose uptake systems supports bifidobacteria-infant symbiosis. *Science Advances*. 5:1-16.
42. Sela DA, Chapman J, Adeuya A, Kim JH, Chen F, et al. 2008. The genome sequence of *Bifidobacterium longum* subsp. *infantis* reveals adaptations for milk utilization within the infant microbiome. *Proceedings of the National Academy of Sciences*. 105:18964-18969.
43. Shani GI, Lewis ZT, Robinson AM, Mills DA. 2018. Interactions between bifidobacteria, milk oligosaccharides, and neonate hosts, p 165-175. 2018. *In* Mattarelli P, Biavati B, Holzaphel WH, Wood BJB (eds), *The Bifidobacteria and Related Organisms*, Academic Press - Elsevier, London UK.
44. Shepherd ES, Deloache WC, Pruss KM, Whitaker WR, Sonnenburg JL. 2018. An exclusive metabolic niche enables strain engraftment in the gut microbiota. *Nature*. 557:434-438.
45. Smilowitz JT, O'Sullivan A, Barile D, German JB, Lönnerdal B, et al. 2013. The human milk metabolome reveals diverse oligosaccharide profiles. *Journal of Nutrition*. 143:1709-1718.
46. Sonnenburg ED, Smits SA, Tikhonov M, Higginbottom SK, Wingreen NS, et al. 2016. Diet-induced extinctions in the gut microbiota compound over generations. *Nature*. 529:212-215.
47. Sonnenburg ED, Sonnenburg JL. 2014. Starving our microbial self: the deleterious consequences of a diet deficient in microbiota-accessible carbohydrates. *Cell Metabolism*. 20:779-786.
48. Suez J, Zmora N, Zilberman-Schapira G, Mor U, Dori-Bachash M, et al. 2018. Post-antibiotic gut mucosal microbiome reconstitution is impaired by probiotics and improved by autologous FMT. *Cell*. 174:1406-1423.
49. Sung V, D'Amico F, Cabana MD, Chau K, Koren G, et al. 2018. *Lactobacillus reuteri* to treat infant colic: a meta-analysis. *Pediatrics*. 141:e20171811.
50. Taft DH, Liu J, Maldonado-Gómez MX, Akre S, Huda MN, et al. 2018. Bifidobacterial dominance of the gut in early life and acquisition of antimicrobial resistance. *mSphere*. 3:1-24.
51. Tissier H. 1900. Recherchés sur la flore intestinale des nourrissons (État normal et pathologique). *Thèse de médecine de l'Université de Paris*. - Paris France.
52. Turroni F, Marchesi JR, Foroni E, Gueimonde M, Shanahan F, et al. 2009. Microbiomic analysis of the bifidobacterial population in the human distal gut. *ISME Journal*. 3:745-751.
53. Turroni F, Milani C, Duranti S, Ferrario C, Lugli GA, et al. 2018. Bifidobacteria and the infant gut: an example of co-evolution and natural selection. *Cell and Molecular Life Sciences*. 75:103-118.
54. Turroni F, Milani C, Duranti S, Mancabelli L, Mangifesta M, et al. 2016. Deciphering bifidobacterial-

mediated metabolic interactions and their impact on gut microbiota by a multi-omics approach. *ISME Journal*. 10:1656-1668.

55. Turroni F, Milani C, van Sinderen D, Ventura M. 2018. Bifidobacteria: ecology and coevolution with the host, p 213-220. *In* Mattarelli P, Biavati B, Holzaphel WH, Wood BJB (eds), *The Bifidobacteria and Related Organisms*, Academic Press - Elsevier, London UK.
56. Turroni F, Peano C, Pass DA, Foroni E, Severgnini M, et al. 2012. Diversity of bifidobacteria within the infant gut microbiota. *PLoS One*. 7:20-24.
57. Underwood MA, Kalanetra KM, Bokulich NA, Lewis ZT, Mirmiran M, et al. 2013. A comparison of two probiotic strains of bifidobacteria in premature infants. *Journal of Pediatrics*. 163:1585-1591.
58. van Best N, Trepels-Kottek S, Savelkoul P, Orlikowsky T, Hornef MW, et al. 2020. Influence of probiotic supplementation on the developing microbiota in human preterm neonates. *Gut Microbes*. 12:1-16.
59. Vatanen T, Franzosa EA, Schwager R, Tripathi S, Arthur TD, et al. 2018. The human gut microbiome in early-onset type 1 diabetes from the TEDDY study. *Nature*. 562:589-594.
60. Vatanen T, Kostic AD, d'Hennezel E, Siljander H, Franzosa EA, et al. 2016. Variation in microbiome LPS immunogenicity contributes to autoimmunity in humans. *Cell*. 165:842-853.

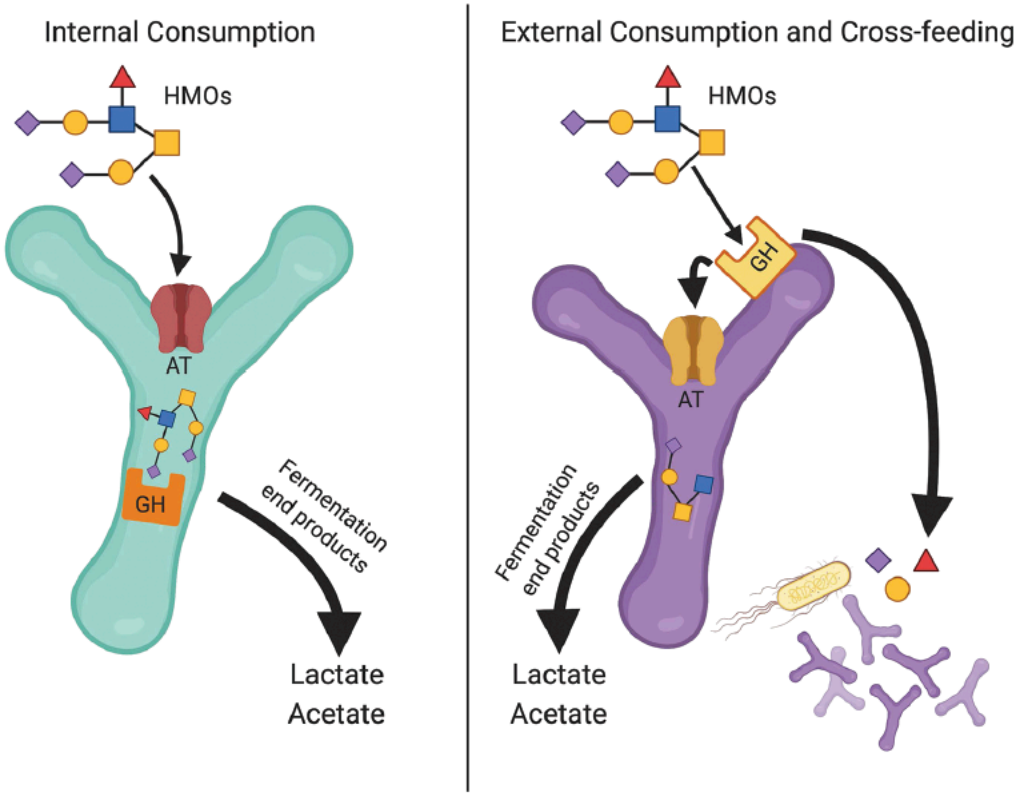

Figure 1.1: Modes of *Bifidobacterium* HMO consumption. Left: Many *Bifidobacterium* species, including *B. longum* subsp. *infantis*, use transporters (such as ABC transporters) to import intact human milk oligosaccharide (HMO) molecules. These bifidobacteria primarily encode internal glycoside hydrolases (GHs) to degrade the HMOs, allowing the bacteria to ferment these carbohydrates into the bioactive end products lactate and acetate. In this mode of consumption, entire HMO molecules are sequestered and metabolized. Right: Other *Bifidobacterium* species, such as *B. bifidum*, encode extracellular GHs that break up HMOs into smaller components which are then imported by transporters. These bifidobacteria also partially ferment HMOs into lactate and acetate. However, this mode of consumption releases small sugars into the gut environment, where they are metabolized by other microbes in a process termed “cross-feeding.” These other microbes may include both bifidobacteria and potential pathogens such as Enterobacteriaceae. HMOs = human milk oligosaccharides. GH = glycoside hydrolase. AT = ABC transporter.

Chapter 2

Dietary Fiber Monosaccharide Content Alters Gut Microbiome Composition and Fermentation *In Vitro*

2.1 Introduction

The human diet primarily comprises fats, proteins, and carbohydrates, with the latter macronutrient contributing the majority of calories in most societies [1]. Besides starches and sugars that are readily digested by mammals, dietary carbohydrate sources include various types of indigestible fiber [2]. Though molecules such as cellulose are relatively inert, many other types of dietary fiber act as “microbiota-accessible carbohydrates” (MACs), which serve as substrates for metabolism by the gut microbiota [3]. These carbohydrates are fermented into bioactive end products such as short-chain fatty acids (SCFAs) that may influence host physiology by altering the pH of the intestinal lumen, contributing to energy balance, and regulating transcription in a variety of metabolic and immune cells by signaling via the receptors Ffar2 and Ffar3 [4]. While many dietary plants, including beets, alfalfa, oats, corn, and soy, are recognized as potential sources of MACs [5], the specific chemical structures within these carbohydrates that facilitate microbial metabolism are often unknown.

Knowledge of diet-derived MAC structure is important because distinct carbohydrates are known to influence the composition and function of the mammalian gut microbiota. Many

strains of gut bacteria are predicted to encode specific carbohydrate-binding molecules alongside hundreds of carbohydrate-active enzymes that may recognize specific linkages [6] and whose mechanisms of action may depend on glycan complexity [7] and entail many coordinated steps [8, 9], sometimes performed by multiple species [10, 11]. Gut bacterial genera such as *Bacteroides* and *Prevotella* express diverse glycoside hydrolases (GHs), polysaccharide lyases (PLs), and carbohydrate esterases (CEs), enzymes that are known or predicted to break down distinct polysaccharides, such as xylans, pectin, and arabinogalactans [12, 13]. The expression of carbohydrate-active enzymes varies extensively within genera and species [14]; for example, the species *Bifidobacterium longum* includes the infant-associated *B. longum* subsp. *infantis*, which encodes a gene cluster for metabolizing human milk oligosaccharides (HMOs) [15], as well as adult-associated strains of *B. longum* subsp. *longum* that specialize in plant oligosaccharide metabolism [16]. Certain microbes can be enriched by targeted provision of specific carbohydrate structures, such as acetylated galactoglucomannans [17, 18] and arabino-oligosaccharides [19]. Species of the genus *Bacteroides* are known to compete for multiple glycans, such as arabinan [20], but may coexist due to differences in physicochemical complexity [21] or substrate prioritization [22], illustrating the intimate relationship between carbohydrate structure and microbial ecology.

Despite increasing recognition of carbohydrate structure as a determinant of gut microbial dynamics, the carbohydrate content of many foods remains poorly characterized and the mechanisms of gut microbiome metabolism are only partially elucidated. Starchy plants are staple foods in many human diets, but dietary starch encompasses both soluble amylopectin that is readily digested and five types of resistant starch, which may be microbiota-accessible [23]. MACs from different food sources may differ in their discrete structure in terms of monosaccharide content, chemical linkages, isomerism, chain length, and modifications such as methylation and sulfation, all of which may differentially affect their degradation by specific gut microbial enzymes [24, 25]. Fermentation by the gut microbiota can be impacted by relatively

fine differences in MAC structure, such as arabinoxylans from different kinds of wheat bran [26, 27], the degree of polymerization of oligosaccharides derived from sugar beet pectin [28], and the linkages found in glucans [29]. However, due to the complex physicochemical properties of food carbohydrates [30] and the analytical difficulties of isolating and analyzing glycans [31], the exact composition of most diet-derived MACs is unknown.

In order to address the challenges of studying the fine structure of complex carbohydrates, Carlito Lebrilla's group has recently developed novel approaches based on ultra-performance liquid chromatography and triple-quadrupole mass spectrometry (UPLC-QqQ-MS). These techniques can reveal, in high throughput, the monosaccharide composition of any carbohydrate of interest [32], data that have been collected for more than 800 foods in the "Davis Food Glycopedia" [33]. Precise monosaccharide composition offers a simple, generalizable means of comparison between numerous dietary fibers, permitting the analysis of how dietary carbohydrate structure affects gut microbiome function at an unprecedented scale.

The present study aimed to determine if differences in fiber monosaccharide content influenced the composition and metabolic function of a model gut microbiota. Data from the Lebrilla group, portions of which have been published in the Davis Food Glycopedia, guided the selection of 55 qualitatively diverse fibers with varied monosaccharide content. In order to model mammalian microbiome function *in vitro*, each fiber was fermented over 72 hours in a bioreactor. 16S rRNA gene sequencing was performed in order to identify changes in the microbiome in tandem with measurements of pH and the levels of acidic microbial metabolites such as short-chain fatty acids.

2.2 Materials and Methods

Monosaccharide composition

Fiber monosaccharide composition data were obtained with ultra-high performance liquid chromatography triple quadrupole mass spectrometry, as previously described [32].

Food processing

Foods (Table S2.1) were processed to model mastication prior to digestion. All foods were purchased from local grocers and stored at 4°C prior to processing in the Food Instruction Lab at the Robert Mondavi Institute for Wine and Food Science. Foods with low water content, such as fried seaweed, were ground into a powder using a Vitamix. Foods with high water content, such as fresh apples, were diced and ground into a slurry using a Vitamix. In some cases, water was added to achieve a homogeneous slurry. Addition of water was recorded and accounted for in the *in vitro* digestion calculations. After processing, foods were stored in Quart Ziplock Bags at -20°C until digestion.

***In vitro* digestion of** foods

The *in vitro* protocol to mimic cat digestion was modeled on the INFOGEST protocol, a previously validated human *in vitro* digestion system[34]. The following changes were made to adapt the protocol to the cat digestive system: Simulated salivary fluids (SSF), simulated gastric fluids (SGF), and simulated intestinal fluids (SIF) were adapted from the INFOGEST protocol to match the minerals found in the cat saliva, gastric fluid, and intestinal fluid respectively. In cases where a range of mineral concentrations are common, the average between the minimum and maximum reported values was used. Table S2.1 details the range of mineral concentrations reported as well as the reference materia. Table S2.2 details the final composition of 1.25X SSF, SGF, and SIF used.

In the oral phase, salivary alpha-amylase was removed, given that cats do not secrete the enzyme, and pH was adjusted to 7.5 based on the average pH of cat saliva[35]. The food slurry was mixed with 1.25X SSF, pH of the mixture was adjusted to 7.5, and the final volume was adjusted using DI water for a final ratio of 1:1 food slurry and SSF. The oral bolus was incubated at 37°C with agitation for 2 minutes. To simulate gastric digestion, the oral bolus was mixed with 1.25X SGF, 2,000 U/mL pepsin (Sigma P6887), and adjusted to pH 2.5 using 6M HCl[36]. DI water was added for a final ratio of 1:1 oral bolus and SGF. The gastric fluid was incubated at 37°C with agitation for 3 hours. While gastric emptying time varies by the individual cat and by the type of food eaten, 3 hours was chosen as a standard based on the average gastric emptying time for dry cat food[37]. To simulate intestinal digestion, the gastric chyme was mixed with 1.25X SIF, pancreatin based on trypsin activity at 100 TAME Units/mL (Sigma P7545)[38], 11.5 U/mL amylase (Sigma A6814), and 5 mg/mL bovine bile (Sigma B3883)[35]. The contribution of amylase in cats is very low, given that their diets are rich in protein. However, there is some evidence that amylase secretion in the pancreas increases after prolonged feeding of a high-carbohydrate diet. The amylase concentration was chosen based on the average amylase secretion from 4 healthy adult cats fed a diet containing potato starch for 3 weeks[39]. The pH of the mixture was adjusted to 6.0 using 1M NaOH[36]. The intestinal slurry was incubated at 37°C with agitation for 2.5 hours, a time chosen based on the average intestinal emptying time of the cat[35]. After incubation, the intestinal slurry was immediately frozen at -20°C to halt enzymatic activity and stored until further use.

Dialysis and anthrone assays

Intestinal slurries were dialyzed to remove monosaccharides and excess salts using Biotech Cellulose Ester Dialysis Membranes (31mm flat width, 100–500 D molecular weight cut-off, Catalog No. 888-10723 , Repligen, Waltham, MA) Dialysis membranes were cut to a length of 400 - 550 mm and stored in 1% (v/v) formaldehyde (refreshed every 2-3 rounds of dialysis).

Prior to each use, dialysis membranes were hydrated and rinsed with distilled water. Approximately 110–220 mL of thawed intestinal slurries were pipetted into each dialysis membrane. The filled dialysis membranes were submerged in a 30 L tub containing 22.5 L of distilled water. No more than 14 dialysis tubes (representing ~350 mL of intestinal slurry) were placed into the same dialysis container. Foods were often dialyzed together and groupings were chosen to avoid intestinal slurries with either a high volume, high monosaccharide content, or high salt content being dialyzed together. The dialysis container was stored at 2°C for the duration of dialysis. Twice per day, the water was exchanged with fresh distilled water. After 96 h, the dialyzed intestinal slurries were harvested from the dialysis membranes, placed into Gallon Ziploc Freezer Bags, and stored at -20°C until freeze drying.

Dialyzed intestinal slurries were lyophilized to remove water content using The Scientific Freeze Dryer (4-tray dryer, Medium, Harvest Right, North Salt Lake, UT). The slurries were thawed in a room temperature water bath, then poured into even layers onto freeze dryer trays. Large volumes (>1.5 L) of dialyzed intestinal slurry were freeze dried in multiple batches and homogenized. Freeze drying conditions were: -30°F (-34°C) for 4 h, vacuum off; 35°F (1.7°C) for 3 h, vacuum on; 80°F (26.7°C) for 12 h, vacuum on; 120°F (48.9°C) for 5 h, vacuum on. The material was then held at 120°F (48.9°C) with the vacuum on until it was retrieved from the machine. The lyophilized powder was then homogenized in a coffee grinder and stored in 50 mL conical tubes kept at -20°C. All lyophilized powders were stored in sealed secondary containers with desiccant prior to anthrone assays.

Anthrone assays were performed to determine the total fiber content of the lyophilized powders. A serial dilution of fibers and amylopectin standards were prepared at 0.75mg/mL, 0.6mg/mL, 0.5mg/mL, 0.4mg/mL, 0.25mg/mL, and 0.1mg/mL. 70µL of serially diluted fibers or amylopectin were combined with 140µL of 2mg/mL anthrone in 6M sulfuric acid in 0.5mL strip-tubes. Reactions were run in duplicate. The strip tubes were centrifuged and run in a

Thermocycler at 90°C for 11 min followed by 20°C for 8 min. Samples were transferred to 96-well plates and fluorescence data were obtained with a plate reader The total fiber content of the lyophilized powder was then calculated.

Batch fermentations of fibers

Batch fecal fermentations were conducted in triplicate with 55 unique fibers of subjects and 9 controls for a total of 64 individual fermentations, divided into 9 experiments with 1 control fermentation per experiment. Fermentations were conducted in an anaerobic chamber using a MiniBioReactor Array (MBRA) system [40, 41] in continuous mode. The MBRA system was modified to permit the fermentation of insoluble fibers without clogging the system's tubing. Soluble fibers were dissolved in solution. Insoluble fibers were placed in the main compartment of the fermenter, rather than the source bottles, and wire mesh of a length equal to the width of the waste line was placed around the waste line. Feline fecal samples (provided by Mars, Inc., McLean, VA) were used to inoculate fermentations. Because the fecal microbiome of cats has been found to cluster by both subject and the date of sampling within subjects [42], a single inoculum for all fermentations was created by pooling 10 fecal samples with distinct microbial communities. The fecal inoculum for each fermentation was placed in the anaerobic chamber and 25% m/v fecal slurry were made using previously reduced 1X PBS. Slurries homogenized by vortexing for 5 min and centrifuged at 200 g for 5 minutes to separate large particles. Supernatant was mixed with fermentation media in a 20:80 ratio and incubated for 72 hours with constant stirring, under anaerobic conditions. Experimental fermentation media contained 1% m/v of the fiber of interest. No carbohydrate was added to control fermentations. 1 mL samples were collected after 0, 24, 48, and 72 hours of batch fermentation. pH was immediately measured as samples were retrieved and samples were then preserved at -80°C prior to subsequent analyses (quantification of acidic microbial metabolites and 16S rRNA gene sequencing).

Quantification of acidic microbial metabolites (AMMs)

Derivatization of SCFAs in 96-well plates. A pooled standard solution consisting of 18 carboxylic acid metabolites was prepared in MeOH and serially diluted to concentrations of 0.001 µg/mL to 500 µg/mL. The batch fermentation supernatants were thawed and centrifuged at 13,500 rpm for 5 minutes. The supernatant was then collected and diluted 25-fold in MeOH. An internal standard mixture containing 100 µg/mL of d4-acetic acid, 50 µg/mL of d2-indolepropionic acid and 10 µg/mL of 2-ethylbutyric acid was spiked into all standards and samples at the ratio of 1:10 (v/v). 200 µL of ACN and 100 µL of derivatization reagent containing 20 mM TPP, 20 mM DPDS and 20 mM 2-PA was plated in a 1 mL 96-well plate beforehand. A 10 µL aliquot of standard/sample was added, the plate sealed, and incubated at 60 °C for 10 minutes. The entire procedure was completed in a 4°C cold room to reduce volatile analyte evaporation. After the reaction was complete, the derivatized samples were dried in a miVac concentrator. The dried samples were reconstituted with 50 % MeOH before instrumental analysis.

LC-MS/MS Analysis. Derivatized analytes were analyzed on an Agilent 6495B QqQ MS coupled to an Agilent 1290 Infinity II UHPLC. Separation was performed on an Agilent Poroshell 120 EC-C18 column (2.1 mm x 100 mm, 1.9 µm particle size). Aqueous mobile phase A consisted of 100% nano-pure water. Organic mobile phase B consisted of 1:1 (v/v) ACN/IPA mixture. The following binary gradient was used: 0.00-1.00 min, 5.00% B; 1.00-10.00 min, 5.00-20.00% B; 10.00-11.00 min, 20.00% B; 11.00-15.00 min, 20.00-60.00% B; 15.00-16.00 min, 60.00-5.00% B. 1 µL of sample was injected in each run. The mobile phase flow rate was 0.45 ml / min and the column temperature was set to 45 °C. The Jet Stream Technology (AJS) ESI ion source was operated in positive ion mode with the following parameters: capillary voltage = 1800 V, nozzle voltage = 1500V, gas temperature = 240 °C, gas flow = 20 L / min, nebulizer =

25 psi, sheath gas temperature = 300 °C, sheath gas flow = 9 L / min. Mass spectrometry data was collected under dynamic multiple reaction monitoring (dMRM) mode.

DNA extraction, library prep, and 16S rRNA gene sequencing

Genomic DNA was extracted using Zymobiomics 96 MagBead DNA Kit (Zymo Research, Irvine, CA) with a Kingfisher Flex automated extraction instrument (Thermo Fisher Scientific, Waltham, MA). As previously described [43], the V4 region of the 16S RNA gene was amplified in triplicate with barcoded PCR primers F515 and R806. Amplicons were verified by gel electrophoresis, combined and purified, and sent to the UC Davis Genome Center for library preparation and high throughput 250 paired end sequencing using an Illumina MiSeq. Sequencing run was performed in two batches. A ZymoBIOMICS mock community was used as a positive control.

Bioinformatics

Raw sequencing data were demultiplexed with Sabre [44]. Demultiplexed data were imported into QIIME2-2021.2 [45], where data were quality filtered and reads were processed with DADA2 [46]. After filtering, taxonomy was assigned to reads using a pre-generated naïve Bayes classifier trained on Silva 138 99% OTUs from the 515F/806R region of sequences [47–49], accessed via QIIME2-2021.2 [45]. Reads mapped to the microbial orders Caldalkalibacillales, Rhizobiales, Sphingomonadales, Micrococcales, and Bacilliales were present in three negative controls on one batch 2DNA extraction plate; therefore, contamination was suspected. Contaminant sequences were statistically identified using Decontam (v. 1.1.1) [50] with default settings and pruned from the dataset using phyloseq (v. 1.34.0) [51], resulting in the removal of 1/1854 taxa from batch 1 samples and 21/1854 taxa from batch 2 samples.

Statistical methods

All statistical analyses were completed in R 4.2.0 statistical software [52] and QIIME2-2021.2 [45].

DBSCAN. Fibers were clustered based on unadjusted monosaccharide composition using the clustering algorithm DBSCAN (density-based spatial clustering of applications with noise), as implemented in R with the package dbscan (v. 1.1-10) [53]. Because the data was high-dimensional and little domain knowledge exists for choosing an appropriate value of the ε parameter [54], hierarchical DBSCAN with simplified hierarchy extraction was performed with a value of minPts = 3.

Data filtering and standardization. Multicollinearity among monosaccharides was identified with caret (v. 6.0-92) with a cutoff of absolute correlation > 0.70, which resulted in the monosaccharides fucose, GlcNac, GalNac, and arabinose being filtered from the dataset and excluded from subsequent analyses. Linear dependencies and near-zero variance variables were not detected in monosaccharide data. Values of the retained monosaccharides were multiplied by the mass of fiber (mg) used in fermentations in order to accurately reflect the amount of carbohydrate present in each fermentation. In order to standardize monosaccharide data across fibers, filtered and corrected monosaccharide values were scaled from 0-1 by subtracting the minimum value of each monosaccharide and dividing the result by the difference between the minimum and maximum values for that monosaccharide. The same parameters were used to identify multicollinearity among acidic microbial metabolites (AMMs) with caret, with the exception that a cutoff of an absolute correlation of > 0.50 absolute correlation was applied, resulting in the exclusion of butyric acid, lactic acid, isobutyric acid, valeric acid, isovaleric acid, 2-methyl butyric acid, hexanoic acid, 2-methyl valeric acid, 3-methyl valeric acid, 4-methyl valeric acid, succinic acid, and indole-3-butyric acid from subsequent analyses. AMMs were also scaled from 0-1 using the same scaling function as for monosaccharides.

Hierarchical clustering. Fibers were grouped by hierarchical clustering based on filtered, corrected, and scaled monosaccharide composition data. A distance matrix based on Euclidean distance between monosaccharide values was calculated. Hierarchical clustering was performed with the hclust function in the base R package using both complete and average linkage and Dunn's index was calculated for different values of k to find its maximum value. The heatmap function was used to plot a heatmap of monosaccharide hierarchical clustering results based on complete linkage. Similarly, filtered and scaled AMM data were grouped with hierarchical clustering and visualized with a heatmap using the same parameters as for monosaccharides; however, average values of AMM concentrations were used due to the variation between samples.

Modeling to predict final pH. To assess the effect of monosaccharide composition on final pH, we used a generalized linear model as implemented in the base package of R. Only monosaccharides found to have an absolute correlation below 0.70 with caret were eligible for inclusion. Purposeful selection was used to select the variables to include in the final model. Log or Box–Cox transformations were applied to monosaccharide data that deviated from normality, as assessed with the Shapiro–Wilk test. Pseudocounts were added to variables with values of zero present if a transformation was applied. The final model was compared to one based on total monosaccharide content by the Akaike information criterion (AIC). Using the same approach as described above for monosaccharide composition, a generalized linear model was implemented to assess the effect of final AMM concentrations on final pH. Only AMMs found to have an absolute correlation below 0.50 with caret were eligible for inclusion.

Alpha diversity. After excluding statistically identified contaminants, samples were rarefied without replacement to a depth of 2509 reads using the vegan package (v. 2.5.7) [55], which retained 1,881,750 features (15.56% of features) in 750 samples (92.59% of samples).Rarefied data were used to calculate alpha diversity with the Shannon index using the vegan package

(vegan package (v. 2.6-2) [55]) with default settings. To assess the effect of monosaccharide composition on longitudinal alpha diversity, we used a linear mixed effects (LME) model, as implemented with the lmer function in the package lmerTest (v. 3.1.3) [56]. Bioreactor ID was used as the grouping variable. Alpha diversity was observed to vary at baseline, so baseline alpha diversity was considered as a variable in the model. Day, baseline alpha diversity, and each monosaccharide were considered as fixed effects. Bioreactor ID was considered as a random effect since it was expected that the baseline values and rate of change would differ between fermentations. Log or Box–Cox transformations were considered for variables that deviated from normality, as assessed with the Shapiro–Wilk test. However, these transformations did not improve the normality of monosaccharide data across the entire time course of fermentation, so they were ultimately not applied. A modified form of purposeful selection was used to select the variables to include in the final model. Separate models were evaluated for each monosaccharide and baseline alpha diversity; each of these models included day as a fixed effect and fermenter as a grouping variable. Restricted maximum likelihood was set to FALSE since the models compared different fixed effects. Variables that were significantly associated with alpha diversity were then assessed in a combined model and the assumptions of linearity, homogeneity of variance, and normal residuals were tested. Although a significant result was obtained in the analysis of variance of the squared residuals for bioreactor ID (p-value = 5.374e-12 by Levene's test), the histogram of the residuals did not appear bimodal. Therefore, since a q-q plot showed relatively linear residuals apart from extrema, the results of Levene's test were disregarded, and other variables were added back into the model by purposeful selection. A confidence interval was calculated using the confint function in the base R package.

Beta diversity. Rarefied data were used to analyze beta diversity (between-sample diversity) because read depth varied more than tenfold between samples. A distance matrix based on

Bray–Curtis distance between samples was calculated based on decontaminated 16S rRNA gene sequencing data with the function vegdist in the vegan package (v. 2.5.7) [55]. Bray–Curtis distance was selected as a distance metric instead of weighted or unweighted Unifrac [57] due to the presence of unassigned reads that became outliers if phylogeny was taken into account. Sequencing data were subsetted by day with phyloseq (v. 1.34.0) [51]. Differences in beta diversity by monosaccharide composition were tested with permutational analysis of variance (PERMANOVA), as implemented by the adonis2 command in vegan, which can accommodate continuous variables. A backwards elimination approach was used to select the final variables for each day's model. Ordination with nonmetric multidimensional scaling (NMDS) was performed with the metaMDS command in vegan to visualize day 3 beta diversity data. Ordinations with points colored using a gradient based on fiber monosaccharide content and pH were created with the plotfunctions package (v. 1.4) [58].

Differential abundance. Differential abundance based on monosaccharide composition and AMM concentration was tested with Analysis of Composition of Microbiomes (ANCOM) [59] in QIIME2-2021.2. Because ANCOM requires discrete variables, monosaccharide composition and AMM concentration values were classified into tertiles with the functions quantile and cut in the base R package. Tertiles were chosen over quartiles or quintiles due to the relatively large number of very small values in many variables. 16S rRNA sequencing data were filtered to exclude samples prior to day 3. Taxonomy was collapsed to the genus level. Pseudocounts were due to the presence of zeros in microbiome data. ANCOM was run separately for each monosaccharide and AMM tertiles.

2.3 Results

In order to test the effects of fiber monosaccharide composition on the outcome of gut microbial fermentation, dietary fibers from 55 unique foods previously analyzed by the Lebrilla group were chosen. An inoculum containing a pooled feline fecal sample (see Materials and Methods) was allowed to ferment each fiber in a bioreactor over a period of 72 hours. Modeling revealed significant associations between fiber monosaccharide composition, pH change and microbial diversity, as well as the contribution of individual microbial metabolites to the final pH. The results suggest that specific monosaccharides, such as rhamnose and xylose, significantly influence the diversity of the gut microbiome and the fermentation of dietary carbohydrates.

55 food fibers with known monosaccharide composition (Table S2.3) were selected to represent a diverse range of dietary fruits, vegetables, and starches common in human diets. The relatively large number of fibers analyzed provided a challenge for robust cross-fiber comparisons. We therefore sought to reduce the number of dimensions with clustering analysis. Monosaccharide data provided by the Lebrilla group were multiplied by the mass of fiber used in each experiment and scaled based on their minimum and maximum values. Results of clustering with hierarchical DBSCAN (Fig. S2.1) identified few clusters based on monosaccharide composition, with unbalanced membership and a high degree of noise. Hierarchical clustering (Fig. 2.1) identified a large number of clusters, with Dunn's Index maximized at k=43. Therefore, instead of grouping fibers into clusters, monosaccharide composition was compared directly across fibers.

The monosaccharide composition of each fiber was documented in terms of glucose, galactose, fructose, xylose, arabinose, fucose, rhamnose, glucuronic acid (GlcA), galacturonic acid (GalA), *N*-Acetylglucosamine (GlcNac), *N*-Acetylgalactosamine (GalNac), mannose, allose, and ribose. Some sugars, such as ribose and fucose, were relatively scarce in most food fibers in this dataset, while others, such as glucose, were present in many fibers. Some

monosaccharides were found to exhibit multicollinearity, and the sugars fucose, GlcNac, GalNac and arabinose (absolute correlation > 0.50) were filtered from the dataset. While the data for some monosaccharides was zero-inflated, no monosaccharides were found to have near-zero variance (data not shown).

In order to determine how fiber monosaccharide composition affected fermentation, each fiber was batch fermented in triplicate for a time course of 72 hours in the presence of a pooled feline fecal inoculum. Prior to fermentation, foods were processed to model mastication and exposed to simulated digestive fluids *in vitro* to mimic feline digestion, after which free monosaccharides were removed with dialysis and the total fiber content was measured with anthrone assays (see Materials and Methods) to create a standard concentration of 1% m/v of the fiber of interest in each fermentation. For most fibers, pH decreased over the course of the experiment (Fig. 2.2), indicating that fermentation generally occurred regardless of fiber. However, the mean final pH ranged from 5.14 for kabocha squash flesh to 6.75 for radish bulb, suggesting that this pooled microbial community could not fully ferment all fibers. In order to determine if fiber monosaccharide composition contributed to the observed variance in the extent of fermentation, we modeled the effect of monosaccharide content on the final pH with generalized linear regression (Table 2.1). The resulting model found that glucose content was significantly associated with a lower final pH, while xylose content was significantly associated with a higher final pH. Initial pH was not predictive of final pH, indicating that monosaccharide composition was an important determinant of fermentation. Since glucose was the predominant sugar in most fibers, we assessed if total monosaccharide content was equally predictive of final pH, and found that the more nuanced model was slightly superior (AIC = 53.821 for the model summarized in Table 2.1, AIC = 54.969 for the model based on total monosaccharide content).

Since monosaccharide content was found to influence the final pH of fiber fermentations, we hypothesized that pH differences resulted from variation in the acidic microbial metabolites (AMMs) produced by the gut microbiota during the metabolism of distinct carbohydrate

structures. AMMs include short-chain fatty acids (SCFAs) as well as other fermentation end products such as hexanoic acid, lactic acid and valeric acid. After each 72-hour fermentation, the final levels of 19 AMMs were measured by LC-MS/MS after derivatization (see Materials and Methods). A heatmap based on hierarchical clustering (Fig. 2.3) suggested that AMM levels varied considerably across input fibers, but failed to reveal any meaningful clusters of similar AMM production. 12 AMMs (butyric acid, lactic acid, isobutyric acid, valeric acid, isovaleric acid, 2-methyl butyric acid, hexanoic acid, 2-methyl valeric acid, 3-methyl valeric acid, 4-methyl valeric acid, succinic acid, and indole-3-propionic acid) were found to exhibit multicollinearity and were filtered from the dataset. The remaining AMMs (acetic acid, 2,2-dimethylbutyric acid, glyceric acid, glycolic acid, indole-3-acetic acid (I3A), indole-3-propionic acid (I3P), and propionic acid) were analyzed to determine their contributions to final pH by generalized linear regression (Table 2.2). Acetic acid, propionic acid, and I3A were significantly associated with a lower final pH, while glyceric acid was significantly associated with a higher final pH, supporting our hypothesis that variation in AMM production contributed to differences in post-fermentation pH.

Given that specific members of the pooled gut microbiota differ in their ability to produce AMMs, we next sought to identify how the composition of the initial microbial community changed over the course of fermentation in response to variation in monosaccharide composition. Four samples (0, 24, 48 and 72 hours) were taken from each fermentation for 16S rRNA sequencing. The relative abundance of microbial orders (Fig. 2.4) was generally similar for 0-hour samples, suggesting that the initial conditions of each fermentation did not vary considerably. Differences in relative abundance were apparent between fiber types in 24-72 hour samples, while samples from fermentation of the same fiber appeared relatively similar across both replicates and time points. The alpha diversity (richness and evenness) of microbiome samples was quantified with the Shannon index after rarefaction to a depth of 2509 reads, which retained 1,881,750 features (15.56% of features) in 750 samples (92.59% of

samples). A linear mixed effects model (Table 2.3) found that baseline alpha diversity was not predictive of longitudinal alpha diversity at 24-72 hours. However, xylose was significantly associated with lower alpha diversity while rhamnose, GalA and GlcA were significantly associated with higher alpha diversity, suggesting that the composition of the microbial community changed due to differences in monosaccharide content.

Since differences in alpha diversity may be accompanied by alterations in the structure of the microbiome, we tested for dissimilarity between microbiome samples from different fermentations (beta-diversity). A distance matrix of Bray–Curtis distances between microbiome samples was calculated. Permutational analysis of variance (PERMANOVA) of the Bray–Curtis distance matrix indicated that sequencing run and the content of the monosaccharides glucose, galactose, fructose, rhamnose, GalA, GalNac, mannose and allose were all significantly associated with the dissimilarity of microbiome samples after 72 hours of fermentation (Table 2.4). Results from 24 and 48 hours were similar to those at 72 hours, with GlcA also a significant variable at 24 hours, while sequencing run was the only significant variable at 0 hours (Table S2.4). These results suggest that many monosaccharides independently influenced microbial community structure over the course of fermentation. Ordination with non-metric multidimensional scaling (NMDS) was performed to visualize 72-hour samples according to their Bray–Curtis distances. Ordinations with points colored using a gradient based on fiber monosaccharide content (Fig. 2.5A) generally agreed with PERMANOVA results, suggesting that samples from the fermentation of fibers with high levels of each monosaccharide were often similar, as measured by Bray-Curtis distance. A gradient plot of final pH (Fig. 2.5B) suggested that samples with similar final pH levels also tended to be similar as measured by Bray-Curtis distance.

Since differences in microbiome composition and structure were evident between fermentations, we next sought to identify which specific microbial genera responded to differences in fiber monosaccharide content and contributed to the observed final pH

differences. Quantitative fiber monosaccharide data were classified into tertiles in order to test for differentially abundant taxa with Analysis of Compositions of Microbiomes (ANCOM) ANCOM results at the genus level (Table 2.5) suggest that differences in the content of 11 monosaccharides were associated with significant differences in the relative abundance of 11 microbial genera, including *Lactobacillus*, *Flavonifractor*, and *Lachnospira*. Notably, the genus *Dubosiella* was enriched in fermentations of fibers with higher levels of three monosaccharides: allose, GalNac, and GlcA. Higher GalA content was significantly associated with the relative abundance of three genera: *Libanicoccus*, *Alistipes*, and *Phocea*. In order to determine if any of these genera contributed to observed differences in microbiome function, 72-hour fermentations containing different tertiles of AMMs were also tested for the differential abundance of microbial genera with ANCOM (Table 2.6). Many of the genera found to be significantly associated with fiber monosaccharide content were also significantly associated with the levels of certain AMMs. The genus *Dubosiella* was significantly associated with 2,2-dimethylbutyric acid and glycolic acid. Interestingly, 28 genera were significantly associated with levels of indole-3-propionic acid and 35 genera were significantly associated with levels of propionic acid.

Briefly, we found significant differences in alpha diversity, beta diversity, and microbial community composition after 72 hours of fermentation based on fiber monosaccharide composition. Final pH was significantly associated with both fiber monosaccharide composition and the levels of acidic microbial metabolites.

2.4 Discussion

The composition of the colonic microbiota of mammals is shaped in large part by the ingestion of dietary fibers [60], with glycan complexity determining the extent to which individual microbes can process these polysaccharides or their oligosaccharide components [61]. Complex dietary glycans are known to nourish extended “food chains” in the mammalian gut, with primary degraders such as *Bacteroides* spp. encoding polysaccharide utilization loci (PULs) to recognize and break down specific structures, releasing byproducts that support downstream niches such as secondary degraders and acetogens [62]. Dietary fibers were recently shown to vary in the specificity of the changes they induce in microbial community structure, with simple, common fibers like fructooligosaccharides inducing less dramatic and less selective changes than insoluble, rarer fibers like *β*-glucan [63]. However, though carbohydrates may be studied with a variety of analytical methods, such as ion mobility spectrometry and gas-phase spectroscopy [64], the complexity of food glycans has precluded detailed understanding of their structure. An ultra-high performance liquid chromatography triple quadrupole mass spectrometry approach developed by the Lebrilla group [32] expands on existing methods in both breadth and depth. Examples of the detailed monosaccharide composition data obtained with this method have been published in the Davis Food Glycopedia [33] for hundreds of common dietary carbohydrate sources, offering relevant structural information for numerous studies that examine the impact of diet on the human gut microbiota. Similarities or differences in chemical structure may not be intuitively obvious; for example, hierarchical clustering suggested that the monosaccharide composition of red sweet potato and Japanese sweet potato was relatively distinct, whereas seemingly unrelated food fibers such as buckwheat and radish bulb were clustered together. These examples suggest that qualitative dietary diversity many not reflect underlying structural diversity, with possible ramifications for studies that seek

that unravel the mechanisms by which the gut microbiome responds to broad dietary patterns, such as the Mediterranean diet [65] or whole grain consumption [66].

The present study takes advantage of the data offered by the Lebrilla group's methods and directly links variation in monosaccharide composition to the outcome of fermentation by the gut microbiome. Modeling revealed that glucose content was the most predictable variable of the final pH of fermentation, a result that likely reflects the wide distribution of glucosidases in the mammalian gut microbiome [67, 68]. While a model based on total monosaccharide content performed almost as well as one based on glucose and xylose content, several individual monosaccharides were significantly associated with microbial alpha and beta diversity and community composition, suggesting that total monosaccharide content is inadequate for understanding the nuances of gut microbial fermentation. Metabolism of less abundant monosaccharides may be common but variable; for example, only certain *Bifidobacterium* and *Bacteroides* strains encode sialidases [69], but sialidases and their associated catabolic pathways were found in 80/397 genomes analyzed from the Human Microbiome Project [70]. Modeling found that xylose content was significantly associated with a higher final pH and a lower alpha diversity. This result may reflect a relative paucity of enzymes for metabolizing xylose-containing carbohydrates in the microbiome inoculum. Alternatively, it is possible that xylose metabolism is relatively common, but xylose-rich foods support the growth of a narrower range of microbes due to factors like competition, leading to reduced net fermentation and alpha diversity. This possibility may be more plausible given that common microbes such as *Prevotella* and *Bacteroides* are known to metabolize xylans and arabinoxylans [12, 26, 27], but the fine structure of xylose-containing oligosaccharides may govern antagonistic regulation of bacterial carbohydrate-active enzymes [71] and the ability of secondary degraders to consume xylooligosaccharide breakdown products [61]. Further supporting this possibility, a recent study showed that related *Prevotella* spp. competed for arabinoxylan, with *P. intestinalis* outcompeting *P. rodentium* and *P. muris [72]*. A randomized controlled trial showed that arabinoxylan reduced

LDL and total cholesterol [73], and *Bacteroides* that metabolize arabinoxylans have been shown to release the antioxidant ferulic acid [27, 74], suggesting that gut microbial xylose metabolism may have health ramifications. In contrast to xylose, the less abundant sugars rhamnose, GalA, and GlcA were significantly associated with a higher alpha diversity. Structures containing these rarer monosaccharides may support a higher alpha diversity by providing a higher selectivity [21], creating many unfilled ecological niches. Future research should identify carbohydrate-active enzymes that process structures containing rhamnose, GalA, and GlcA in order to determine which microbes are capable of processing them.

Fermentation pH and microbial diversity were also found to reflect variation in acidic microbial metabolites (AMMs), which are known to affect microbial ecology. While changes in dietary fiber consumption are known to rapidly alter AMM production by the mammalian gut microbiota, such as that of beagles [75], the metabolic fluxes that convert individual dietary monosaccharides into AMMs are poorly understood. A recent study suggested that AMMs such as succinic acid, propionic acid, and butyric acid differentially inhibited gut Bacteroidales, but that sensitivity to butyric acid depended on the provision of specific carbohydrates [76]. Modeling found that final pH was most strongly associated with acetic acid, likely because acetic acid is the most widely produced short-chain fatty acid (SCFA) in the gut (the molar ratio of acetic acid:propionic acid:butyric acid is 60:20:20) [4]. A reduction in mouse cecal pH mediated by the production of acetic acid by *Bifidobacterium* was shown to protect against infection by *E. coli* O157:H7 [77], suggesting that this metabolite is physiologically important for the mammalian host. Modeling also revealed that propionic acid was also significantly associated with a lower final pH, as well as the relative abundance of 35 microbial genera. While propionic acid is less studied than butyric acid and acetic acid, it was found to increase in human subjects fed corn bran arabinoxylan [78] and has been shown to mediate colonization resistance to *Salmonella* infection in a mouse model [79], suggesting that future studies should examine its production by genera identified here, such as *Lactobacillus* and *Romboutsia*.

Propionic acid may be produced by multiple routes, including from succinate and via the acrylate pathway [80], possibly explaining why numerous genera were significantly associated with propionic acid levels. While many studies have examined production of SCFAs by the gut microbiota, the present study highlights the potential importance of a broader range of AMMs. Indole-3-acetic acid (I3A) was also found to be significantly associated with a lower final pH, while indole-3-propionic acid (I3P) was significantly associated with the relative abundance of 28 microbial genera, suggesting that it may be produced by a variety of gut bacteria. These indole derivatives are known to be bioactive: I3P signals through the pregnane X receptor to maintain intestinal barrier integrity [81], while I3A signals via the aryl hydrocarbon receptor (AhR) and may reduce liver inflammation [82]. However, the relationship between host diet, microbial metabolism, and the production of these metabolites remains unclear. While some gut bacteria, such as *Bacteroides* spp. are primary degraders that directly break down food polysaccharides, other bacteria perform “cross-feeding” by taking up the byproducts released by primary degraders [83]. Many AMMs are produced via cross-feeding; for example *Faecalibacterium prausnitzii*, a major butyrate producer, was shown to encode two loci for catabolizing mannooligosaccharides liberated released by primary degradation of *β*-mannans [84]. While our study identified several genera whose relative abundance was significantly associated with monosaccharide content and AMM levels, such associations could be indirect due to interspecific ecological interactions, such as cross-feeding and competition. Future studies should trace the microbial origins of these metabolites in order to establish the foci at which variation in dietary monosaccharide content affects microbial food webs.

The factors that influence both food carbohydrate structure and the ecology of the gut microbiota are multifactorial, so understanding their relationship presents a challenge of immense dimensions. However, the present study suggests that monosaccharide composition provides a generalizable metric for comparing dietary carbohydrates and identifying the functional roles of individual members of the microbiota. The principle of competitive exclusion

suggests that each microbe must realize a distinct niche in the gut ecosystem, but this situation may be achieved by multiple possible mechanisms, such as alternative gene regulation and enzymatic specificity [11]. Microbes may also exhibit metabolic flexibility; in a study manipulating *Bacteroides cellulolyticus* competed with *B. vulgatus* for arabinan, but was relieved of competition for arabinoxylan by *B. ovatus* prioritizing alternate glycans [20]. Despite the complexities of such interactions, monosaccharide composition offers a scalable resource for the large-scale analysis of dietary carbohydrate structure in order to help untangle the mechanisms by which gut bacteria metabolize microbiota-accessible carbohydrates. Although our study used a pooled, feline fecal sample, we demonstrated the reproducibility of a bioreactor-based system for analyzing the response of a mammalian microbiota to a large set of dietary fibers, allowing the impact of carbohydrate structure to be examined independently of host factors. We identified little-studied significant associations between monosaccharide content and the relative abundance of specific genera, such as the significant association between higher GalA content and the relative abundance of *Libanicoccus*, *Alistipes*, and *Phocea*. While *Phocea* and *Libanicoccus* have been isolated from human stool [85, 86], they are poorly studied and may merit further investigation in relation to diet and metabolism. In contrast, the genus *Alistipes* is well-known within the human gut for its bile tolerance [87] and ability to perform protein putrefaction [88], but its response to dietary fibers containing GalA has not been studied. Analysis of monosaccharide composition provides a simple way to identify many such potential links between dietary carbohydrate structure and specific gut bacteria, providing the seed for numerous follow-up studies that test hypotheses and disentangle the mechanisms by which bacteria may metabolize food glycans. Examples to guide such research include past studies that have demonstrated how individual gut bacteria consume human milk oligosaccharides [89], mucins [90, 91], algal porphyrans [10], red seaweed agarose [92], β-mannans [84], and acetylated galactoglucomannans and arabinoglucuronoxylans [18, 93].

Our study thus provides an initial framework for analyzing dietary monosaccharide intake as one of several factors that contribute to the mechanisms of gut microbial metabolism. Future studies may exploit emerging methods, such as chemical and isotopic labeling, in order to trace the fate of individual dietary monosaccharides in single microbial cells [94]. While our work identified monosaccharide content as a determinant of fermentation, future studies should examine other facets of carbohydrate structure that are known to affect microbial metabolism, such as linkages [95] and chemical modifications [25, 96]. A recent study compared the human gut microbiome's response to arabinan-rich pea fiber and homogalacturonan-rich orange fiber *in vivo* and found that changes in carbohydrate-active enzyme content were negatively correlated with the glycosidic linkages they targeted [97], suggesting that monosaccharides should be considered within their broader structural context. More nuanced structural analysis may also use liquid chromatography-mass spectrometry to identify oligosaccharides produced by the cleavage of polysaccharides [98] in order to predict which secondary degraders may be able to exploit the breakdown of a dietary glycans. Fiber monosaccharide data may provide input for deep learning algorithms to predict microbial responses to diet [99]. Eventually, knowledge of the intimate relationships between carbohydrate structure and the metabolism of individual microbes may permit the development of more tailored "microbiota-directed foods" [100] that target functional outcomes, such as the production of bioactive microbial metabolites or changes in the host's plasma proteome [101]. A recent human crossover trial found that butyrate production by the gut microbiota in response to the simple glycans inulin, galactooligosaccharides (GOS), and dextrin was limited by an individual's habitual fiber intake [102], suggesting that future interventions may be more successful if they exploit a deeper understanding of dietary fiber structure to identify personal gaps in the structural diversity of human diets.

2.5 Conclusion

55 food-derived fibers were batch fermented by a feline fecal inoculum over 72 hours in a MiniBioReactor Array (MBRA) system. The extent of pH decrease during each fermentation was significantly associated with the monosaccharides glucose and xylose and the acidic microbial metabolites (AMMs) acetic acid, propionic acid, glyceric acid, and indole-3-acetic acid (I3A). Fecal microbiome diversity and composition were also significantly associated with monosaccharide composition and AMM concentrations, with the content of the monosaccharides xylose, rhamnose, GlcA, and GalA predicting longitudinal alpha diversity.

ACKNOWLEDGEMENT OF WORK

This project was a multidisciplinary effort and I thank everyone in the Mills and Lebrilla laboratories, without whom this research could not have been completed. Monosaccharide composition data were collected by Juan Castillo, Garret Couture, and other members of the Lebrilla laboratory. Dr. María X. Maldonado-Gómez developed the modified MiniBioReactor Array (MBRA) system and oversaw food processing, *in vitro* digestion, and batch fermentations, which she conducted with Nithya Kumar and Dale Koch. Acidic microbial metabolite (AMM) data were collected by Charlie Weng of the Lebrilla laboratory. Dr. Karen Kalanetra demultiplexed 16S rRNA gene sequencing data and provided advice and support on bioinformatics. Dr. Diana Taft assisted with DNA extraction and provided extensive advice and support throughout bioinformatics and statistical analysis.

REFERENCES

1. Schmidhuber J, Sur P, Fay K, Huntley B, Salama J, Lee A, et al. The Global Nutrient Database: availability of macronutrients and micronutrients in 195 countries from 1980 to 2013. Lancet Planet Health. 2018;2:e353–68.

2. Slavin J, Carlson J. Carbohydrates. Adv Nutr. 2014;5:760–1.

3. Sonnenburg ED, Sonnenburg JL. Starving our microbial self: the deleterious consequences of a diet deficient in microbiota-accessible carbohydrates. Cell Metab. 2014;20:779–86.

4. den Besten G, van Eunen K, Groen AK, Venema K, Reijngoud D-J, Bakker BM. The role of short-chain fatty acids in the interplay between diet, gut microbiota, and host energy metabolism. J Lipid Res. 2013;54:2325–40.

5. Sonnenburg ED, Smits SA, Tikhonov M, Higginbottom SK, Wingreen NS, Sonnenburg JL. Diet-induced extinctions in the gut microbiota compound over generations. Nature. 2016;529:212–5.

6. Flint HJ, Scott KP, Duncan SH, Louis P, Forano E. Microbial degradation of complex carbohydrates in the gut. Gut Microbes. 2012;3:289–306.

7. Ndeh D, Gilbert HJ. Biochemistry of complex glycan depolymerisation by the human gut microbiota. FEMS Microbiol Rev. 2018;42:146–64.

8. Luis AS, Briggs J, Zhang X, Farnell B, Ndeh D, Labourel A, et al. Dietary pectic glycans are degraded by coordinated enzyme pathways in human colonic Bacteroides. Nat Microbiol. 2018;3:210–9.

9. La Rosa SL, Ostrowski MP, Vera-Ponce de León A, McKee LS, Larsbrink J, Eijsink VG, et al. Glycan processing in gut microbiomes. Curr Opin Microbiol. 2022;67:102143.

10. Robb CS, Hobbs JK, Pluvinage B, Reintjes G, Klassen L, Monteith S, et al. Metabolism of a hybrid algal galactan by members of the human gut microbiome. Nat Chem Biol. 2022;18:501–10.

11. Lindemann SR. A piece of the pie: engineering microbiomes by exploiting division of labor in complex polysaccharide consumption. Curr Opin Chem Eng. 2020;30:96–102.

12. Aakko J, Pietilä S, Toivonen R, Rokka A, Mokkala K, Laitinen K, et al. A carbohydrate-active enzyme (CAZy) profile links successful metabolic specialization of Prevotella to its abundance in gut microbiota. Sci Rep. 2020;10:12411.

13. Cartmell A, Muñoz-Muñoz J, Briggs JA, Ndeh DA, Lowe EC, Baslé A, et al. A surface endogalactanase in Bacteroides thetaiotaomicron confers keystone status for arabinogalactan degradation. Nat Microbiol. 2018;3:1314–26.

14. Chung WSF, Walker AW, Louis P, Parkhill J, Vermeiren J, Bosscher D, et al. Modulation of the human gut microbiota by dietary fibres occurs at the species level. BMC Biol. 2016;14:3.

15. Sela DA, Chapman J, Adeuya A, Kim JH, Chen F, Whitehead TR, et al. The genome sequence of Bifidobacterium longum subsp. infantis reveals adaptations for milk utilization within the infant microbiome. Proc Natl Acad Sci USA. 2008;105:18964–9.

16. Lee J-H, O'Sullivan DJ. Genomic insights into bifidobacteria. Microbiol Mol Biol Rev.

2010;74:378–416.

17. Michalak L, Gaby JC, Lagos L, La Rosa SL, Terrapon N, Lombard V, et al. Engineered fibre enables targeted activation of butyrate producing microbiota in the distal gut. BioRxiv. 2019.

18. Michalak L, Gaby JC, Lagos L, La Rosa SL, Hvidsten TR, Tétard-Jones C, et al. Microbiota-directed fibre activates both targeted and secondary metabolic shifts in the distal gut. Nat Commun. 2020;11:5773.

19. Holck J, Lorentzen A, Vigsnæs LK, Licht TR, Mikkelsen JD, Meyer AS. Feruloylated and nonferuloylated arabino-oligosaccharides from sugar beet pectin selectively stimulate the growth of Bifidobacterium spp. in human fecal in vitro fermentations. J Agric Food Chem. 2011;59:6511–9.

20. Patnode ML, Beller ZW, Han ND, Cheng J, Peters SL, Terrapon N, et al. Interspecies Competition Impacts Targeted Manipulation of Human Gut Bacteria by Fiber-Derived Glycans. Cell. 2019;179:59-73.e13.

21. Cantu-Jungles TM, Hamaker BR. New view on dietary fiber selection for predictable shifts in gut microbiota. MBio. 2020;11.

22. Tuncil YE, Xiao Y, Porter NT, Reuhs BL, Martens EC, Hamaker BR. Reciprocal prioritization to dietary glycans by gut bacteria in a competitive environment promotes stable coexistence. MBio. 2017;8.

23. Cerqueira FM, Photenhauer AL, Pollet RM, Brown HA, Koropatkin NM. Starch digestion by gut bacteria: crowdsourcing for carbs. Trends Microbiol. 2020;28:95–108.

24. Hamaker BR, Tuncil YE. A perspective on the complexity of dietary fiber structures and their potential effect on the gut microbiota. J Mol Biol. 2014;426:3838–50.

25. Munoz-Munoz J, Ndeh D, Fernandez-Julia P, Walton G, Henrissat B, Gilbert HJ. Sulfation of Arabinogalactan Proteins Confers Privileged Nutrient Status to Bacteroides plebeius. MBio. 2021;12:e0136821.

26. Tuncil YE, Thakkar RD, Arioglu-Tuncil S, Hamaker BR, Lindemann SR. Subtle Variations in Dietary-Fiber Fine Structure Differentially Influence the Composition and Metabolic Function of Gut Microbiota. mSphere. 2020;5.

27. Pereira GV, Abdel-Hamid AM, Dutta S, D'Alessandro-Gabazza CN, Wefers D, Farris JA, et al. Degradation of complex arabinoxylans by human colonic Bacteroidetes. Nat Commun. 2021;12:459.

28. Holck J, Hjernø K, Lorentzen A, Vigsnæs LK, Hemmingsen L, Licht TR, et al. Tailored enzymatic production of oligosaccharides from sugar beet pectin and evidence of differential effects of a single DP chain length difference on human faecal microbiota composition after in vitro fermentation. Process Biochemistry. 2011;46:1039–49.

29. Romero Marcia AD, Yao T, Chen M-H, Oles RE, Lindemann SR. Fine carbohydrate structure of dietary resistant glucans governs the structure and function of human gut microbiota. Nutrients. 2021;13.

30. Cummings JH, Stephen AM. Carbohydrate terminology and classification. Eur J Clin Nutr. 2007;61 Suppl 1:S5-18.

31. Cummings RD, Pierce JM. The challenge and promise of glycomics. Chem Biol. 2014;21:1–

15.

32. Amicucci MJ, Galermo AG, Nandita E, Vo T-TT, Liu Y, Lee M, et al. A rapid-throughput adaptable method for determining the monosaccharide composition of polysaccharides. Int J Mass Spectrom. 2019;438:22–8.

33. Castillo JJ, Couture G, Bacalzo NP, Chen Y, Chin EL, Blecksmith SE, et al. The Development of the Davis Food Glycopedia-A Glycan Encyclopedia of Food. Nutrients. 2022;14.

34. Brodkorb A, Egger L, Alminger M, Alvito P, Assunção R, Ballance S, et al. INFOGEST static in vitro simulation of gastrointestinal food digestion. Nat Protoc. 2019;14:991–1014.

35. Council NR, Division on Earth and Life Studies, Board on Agriculture and Natural Resources, Committee on Animal Nutrition, Subcommittee on Dog and Cat Nutrition. Nutrient Requirements of Dogs and Cats. illustrated, reprint, revised edition. National Academies Press; 2006.

36. Brosey BP, Hill RC, Scott KC. Gastrointestinal volatile fatty acid concentrations and pH in cats. Am J Vet Res. 2000;61:359–61.

37. Wyse CA, McLellan J, Dickie AM, Sutton DGM, Preston T, Yam PS. A review of methods for assessment of the rate of gastric emptying in the dog and cat: 1898-2002. J Vet Intern Med. 2003;17:609–21.

38. Case RM, Harper AA, Scratcherd T. The secretion of electrolytes and enzymes by the pancreas of the anaesthetized cat. J Physiol (Lond). 1969;201:335–48.

39. Kienzle E. Carbohydrate metabolism of the cat 1. Activity of amylase in the gastrointestinal tract of the cat. J Anim Physiol Anim Nutr (Berl). 1993;69:92–101.

40. Hobson CA, Vigue L, Naimi S, Chassaing B, Magnan M, Bonacorsi S, et al. MiniBioReactor Array (MBRA) in vitro gut model: a reliable system to study microbiota-dependent response to antibiotic treatment. JAC Antimicrob Resist. 2022;4:dlac077.

41. Auchtung JM, Robinson CD, Britton RA. Cultivation of stable, reproducible microbial communities from different fecal donors using minibioreactor arrays (MBRAs). Microbiome. 2015;3:42.

42. Bosch G, Heesen L, de Melo Santos K, Pellikaan WF, Cone JW, Hendriks WH. Evaluation of an in vitro fibre fermentation method using feline faecal inocula: repeatability and reproducibility. J Nutr Sci. 2017;6:e25.

43. Lewis ZT, Totten SM, Smilowitz JT, Popovic M, Parker E, Lemay DG, et al. Maternal fucosyltransferase 2 status affects the gut bifidobacterial communities of breastfed infants. Microbiome. 2015;3:13.

44. Joshi N. sabre - A Barcode Demultiplexing and Trimming Tool for FastQ Files. Computer software. GitHub; 2016.

45. Bolyen E, Rideout JR, Dillon MR, Bokulich NA, Abnet CC, Al-Ghalith GA, et al. Reproducible, interactive, scalable and extensible microbiome data science using QIIME 2. Nat Biotechnol. 2019;37:852–7.

46. Callahan BJ, McMurdie PJ, Rosen MJ, Han AW, Johnson AJA, Holmes SP. DADA2: High-resolution sample inference from Illumina amplicon data. Nat Methods. 2016;13:581–3.

47. Bokulich NA, Kaehler BD, Rideout JR, Dillon M, Bolyen E, Knight R, et al. Optimizing taxonomic classification of marker-gene amplicon sequences with QIIME 2's q2-feature-classifier plugin. Microbiome. 2018;6:90.

48. Quast C, Pruesse E, Yilmaz P, Gerken J, Schweer T, Yarza P, et al. The SILVA ribosomal RNA gene database project: improved data processing and web-based tools. Nucleic Acids Res. 2013;41 Database issue:D590-6.

49. Robeson MS, O'Rourke DR, Kaehler BD, Ziemski M, Dillon MR, Foster JT, et al. RESCRIPt: Reproducible sequence taxonomy reference database management. PLoS Comput Biol. 2021;17:e1009581.

50. Davis NM, Proctor D, Holmes SP, Relman DA, Callahan BJ. Simple statistical identification and removal of contaminant sequences in marker-gene and metagenomics data. BioRxiv. 2017.

51. McMurdie PJ, Holmes S. phyloseq: an R package for reproducible interactive analysis and graphics of microbiome census data. PLoS ONE. 2013;8:e61217.

52. R Core Team. R: A language and environment for statistical computing. Computer software. R Foundation for Statistical Computing, Vienna, Austria; 2022.

53. Hahsler M, Piekenbrock M, Doran D. dbscan : Fast Density-Based Clustering with *R*. J Stat Softw. 2019;91.

54. Schubert E, Sander J, Ester M, Kriegel HP, Xu X. DBSCAN Revisited, Revisited. ACM Trans Database Syst. 2017;42:1–21.

55. Oksanen J, Simpson GL, Blanchet FG, Kindt R, Legendre P, Minchin PR, et al. vegan: Community Ecology Package. Computer software. CRAN; 2021.

56. Kuznetsova A, Brockhoff PB, Christensen RHB. lmertest package: tests in linear mixed effects models. J Stat Softw. 2017;82:1–26.

57. Lozupone CA, Hamady M, Kelley ST, Knight R. Quantitative and qualitative beta diversity measures lead to different insights into factors that structure microbial communities. Appl Environ Microbiol. 2007;73:1576–85.

58. van Rij J. plotfunctions: Various Functions to Facilitate Visualization of Data and Analysis. Computer software. CRAN; 2020.

59. Mandal S, Van Treuren W, White RA, Eggesbø M, Knight R, Peddada SD. Analysis of composition of microbiomes: a novel method for studying microbial composition. Microb Ecol Health Dis. 2015;26:27663.

60. Makki K, Deehan EC, Walter J, Bäckhed F. The impact of dietary fiber on gut microbiota in host health and disease. Cell Host Microbe. 2018;23:705–15.

61. Rogowski A, Briggs JA, Mortimer JC, Tryfona T, Terrapon N, Lowe EC, et al. Glycan complexity dictates microbial resource allocation in the large intestine. Nat Commun. 2015;6:7481.

62. Koropatkin NM, Cameron EA, Martens EC. How glycan metabolism shapes the human gut microbiota. Nat Rev Microbiol. 2012;10:323–35.

63. Cantu-Jungles TM, Bulut N, Chambry E, Ruthes A, Iacomini M, Keshavarzian A, et al. Dietary fiber hierarchical specificity: the missing link for predictable and strong shifts in gut bacterial communities. MBio. 2021;12:e0102821.

64. Grabarics M, Lettow M, Kirschbaum C, Greis K, Manz C, Pagel K. Mass Spectrometry-Based Techniques to Elucidate the Sugar Code. Chem Rev. 2022;122:7840–908.

65. De Filippis F, Pellegrini N, Vannini L, Jeffery IB, La Storia A, Laghi L, et al. High-level adherence to a Mediterranean diet beneficially impacts the gut microbiota and associated metabolome. Gut. 2016;65:1812–21.

66. Roager HM, Vogt JK, Kristensen M, Hansen LBS, Ibrügger S, Mærkedahl RB, et al. Whole grain-rich diet reduces body weight and systemic low-grade inflammation without inducing major changes of the gut microbiome: a randomised cross-over trial. Gut. 2019;68:83–93.

67. El Kaoutari A, Armougom F, Gordon JI, Raoult D, Henrissat B. The abundance and variety of carbohydrate-active enzymes in the human gut microbiota. Nat Rev Microbiol. 2013;11:497–504.

68. Wardman JF, Bains RK, Rahfeld P, Withers SG. Carbohydrate-active enzymes (CAZymes) in the gut microbiome. Nat Rev Microbiol. 2022.

69. Coker JK, Moyne O, Rodionov DA, Zengler K. Carbohydrates great and small, from dietary fiber to sialic acids: How glycans influence the gut microbiome and affect human health. Gut Microbes. 2021;13:1–18.

70. Ravcheev DA, Thiele I. Comparative Genomic Analysis of the Human Gut Microbiome Reveals a Broad Distribution of Metabolic Pathways for the Degradation of Host-Synthetized Mucin Glycans and Utilization of Mucin-Derived Monosaccharides. Front Genet. 2017;8:111.

71. Mendis M, Martens EC, Simsek S. How fine structural differences of xylooligosaccharides and arabinoxylooligosaccharides regulate differential growth of bacteroides species. J Agric Food Chem. 2018;66:8398–405.

72. Gálvez EJC, Iljazovic A, Amend L, Lesker TR, Renault T, Thiemann S, et al. Distinct Polysaccharide Utilization Determines Interspecies Competition between Intestinal Prevotella spp. Cell Host Microbe. 2020;28:838-852.e6.

73. Lancaster SM, Lee-McMullen B, Abbott CW, Quijada JV, Hornburg D, Park H, et al. Global, distinctive, and personal changes in molecular and microbial profiles by specific fibers in humans. Cell Host Microbe. 2022;30:848-862.e7.

74. Yasuma T, Toda M, Abdel-Hamid AM, D'Alessandro-Gabazza C, Kobayashi T, Nishihama K, et al. Degradation Products of Complex Arabinoxylans by Bacteroides intestinalis Enhance the Host Immune Response. Microorganisms. 2021;9.

75. Lin C-Y, Jha AR, Oba PM, Yotis SM, Shmalberg J, Honaker RW, et al. Longitudinal fecal microbiome and metabolite data demonstrate rapid shifts and subsequent stabilization after an abrupt dietary change in healthy adult dogs. Anim Microbiome. 2022;4:46.

76. Park S-Y, Rao C, Coyte KZ, Kuziel GA, Zhang Y, Huang W, et al. Strain-level fitness in the gut microbiome is an emergent property of glycans and a single metabolite. Cell. 2022;185:513-529.e21.

77. Fukuda S, Toh H, Hase K, Oshima K, Nakanishi Y, Yoshimura K, et al. Bifidobacteria can protect from enteropathogenic infection through production of acetate. Nature. 2011;469:543–7.

78. Nguyen NK, Deehan EC, Zhang Z, Jin M, Baskota N, Perez-Muñoz ME, et al. Gut microbiota modulation with long-chain corn bran arabinoxylan in adults with overweight and obesity is linked to an individualized temporal increase in fecal propionate. Microbiome.

2020;8:118.

79. Jacobson A, Lam L, Rajendram M, Tamburini F, Honeycutt J, Pham T, et al. A Gut Commensal-Produced Metabolite Mediates Colonization Resistance to Salmonella Infection. Cell Host Microbe. 2018;24:296-307.e7.

80. Louis P, Scott KP, Duncan SH, Flint HJ. Understanding the effects of diet on bacterial metabolism in the large intestine. J Appl Microbiol. 2007;102:1197–208.

81. Venkatesh M, Mukherjee S, Wang H, Li H, Sun K, Benechet AP, et al. Symbiotic bacterial metabolites regulate gastrointestinal barrier function via the xenobiotic sensor PXR and Toll-like receptor 4. Immunity. 2014;41:296–310.

82. Krishnan S, Ding Y, Saedi N, Choi M, Sridharan GV, Sherr DH, et al. Gut Microbiota-Derived Tryptophan Metabolites Modulate Inflammatory Response in Hepatocytes and Macrophages. Cell Rep. 2018;23:1099–111.

83. Flint HJ, Duncan SH, Louis P. The impact of nutrition on intestinal bacterial communities. Curr Opin Microbiol. 2017;38:59–65.

84. Lindstad LJ, Lo G, Leivers S, Lu Z, Michalak L, Pereira GV, et al. Human Gut Faecalibacterium prausnitzii Deploys a Highly Efficient Conserved System To Cross-Feed on β-Mannan-Derived Oligosaccharides. MBio. 2021;12:e0362820.

85. Bilen M, Cadoret F, Richez M, Tomei E, Daoud Z, Raoult D, et al. Libanicoccus massiliensis gen. nov., sp. nov., a new bacterium isolated from human stool. New Microbes New Infect. 2018;21:63–71.

86. Ndongo S, Lagier JC, Fournier PE, Raoult D, Khelaifia S. “Phocea massiliensis” a new bacterial species isolated from the human gut. New Microbes New Infect. 2016;13:67–8.

87. David LA, Maurice CF, Carmody RN, Gootenberg DB, Button JE, Wolfe BE, et al. Diet rapidly and reproducibly alters the human gut microbiome. Nature. 2014;505:559–63.

88. Parker BJ, Wearsch PA, Veloo ACM, Rodriguez-Palacios A. The genus alistipes: gut bacteria with emerging implications to inflammation, cancer, and mental health. Front Immunol. 2020;11:906.

89. Marcobal A, Barboza M, Sonnenburg ED, Pudlo N, Martens EC, Desai P, et al. Bacteroides in the infant gut consume milk oligosaccharides via mucus-utilization pathways. Cell Host Microbe. 2011;10:507–14.

90. Crouch LI, Liberato MV, Urbanowicz PA, Baslé A, Lamb CA, Stewart CJ, et al. Prominent members of the human gut microbiota express endo-acting O-glycanases to initiate mucin breakdown. Nat Commun. 2020;11:4017.

91. Bell A, Juge N. Mucosal glycan degradation of the host by the gut microbiota. Glycobiology. 2021;31:691–6.

92. Yun EJ, Yu S, Park NJ, Cho Y, Han NR, Jin Y-S, et al. Metabolic and enzymatic elucidation of cooperative degradation of red seaweed agarose by two human gut bacteria. Sci Rep. 2021;11:13955.

93. La Rosa SL, Kachrimanidou V, Buffetto F, Pope PB, Pudlo NA, Martens EC, et al. Wood-Derived Dietary Fibers Promote Beneficial Human Gut Microbiota. mSphere. 2019;4.

94. Klassen L, Xing X, Tingley JP, Low KE, King ML, Reintjes G, et al. Approaches to

investigate selective dietary polysaccharide utilization by human gut microbiota at a functional level. Front Microbiol. 2021;12:632684.

95. Galermo AG, Nandita E, Castillo JJ, Amicucci MJ, Lebrilla CB. Development of an extensive linkage library for characterization of carbohydrates. Anal Chem. 2019;91:13022–31.

96. Luis AS, Baslé A, Byrne DP, Wright GSA, London JA, Jin C, et al. Sulfated glycan recognition by carbohydrate sulfatases of the human gut microbiota. Nat Chem Biol. 2022.

97. Delannoy-Bruno O, Desai C, Castillo JJ, Couture G, Barve RA, Lombard V, et al. An approach for evaluating the effects of dietary fiber polysaccharides on the human gut microbiome and plasma proteome. Proc Natl Acad Sci USA. 2022;119:e2123411119.

98. Amicucci MJ, Nandita E, Galermo AG, Castillo JJ, Chen S, Park D, et al. A nonenzymatic method for cleaving polysaccharides to yield oligosaccharides for structural analysis. Nat Commun. 2020;11:3963.

99. Bojar D, Powers RK, Camacho DM, Collins JJ. Deep-Learning Resources for Studying Glycan-Mediated Host-Microbe Interactions. Cell Host Microbe. 2021;29:132-144.e3.

100. Barratt MJ, Lebrilla C, Shapiro H-Y, Gordon JI. The gut microbiota, food science, and human nutrition: A timely marriage. Cell Host Microbe. 2017;22:134–41.

101. Delannoy-Bruno O, Desai C, Raman AS, Chen RY, Hibberd MC, Cheng J, et al. Evaluating microbiome-directed fibre snacks in gnotobiotic mice and humans. Nature. 2021;595:91–5.

102. Holmes ZC, Villa MM, Durand HK, Jiang S, Dallow EP, Petrone BL, et al. Microbiota responses to different prebiotics are conserved within individuals and associated with habitual fiber intake. Microbiome. 2022;10:114.

Figures and Tables

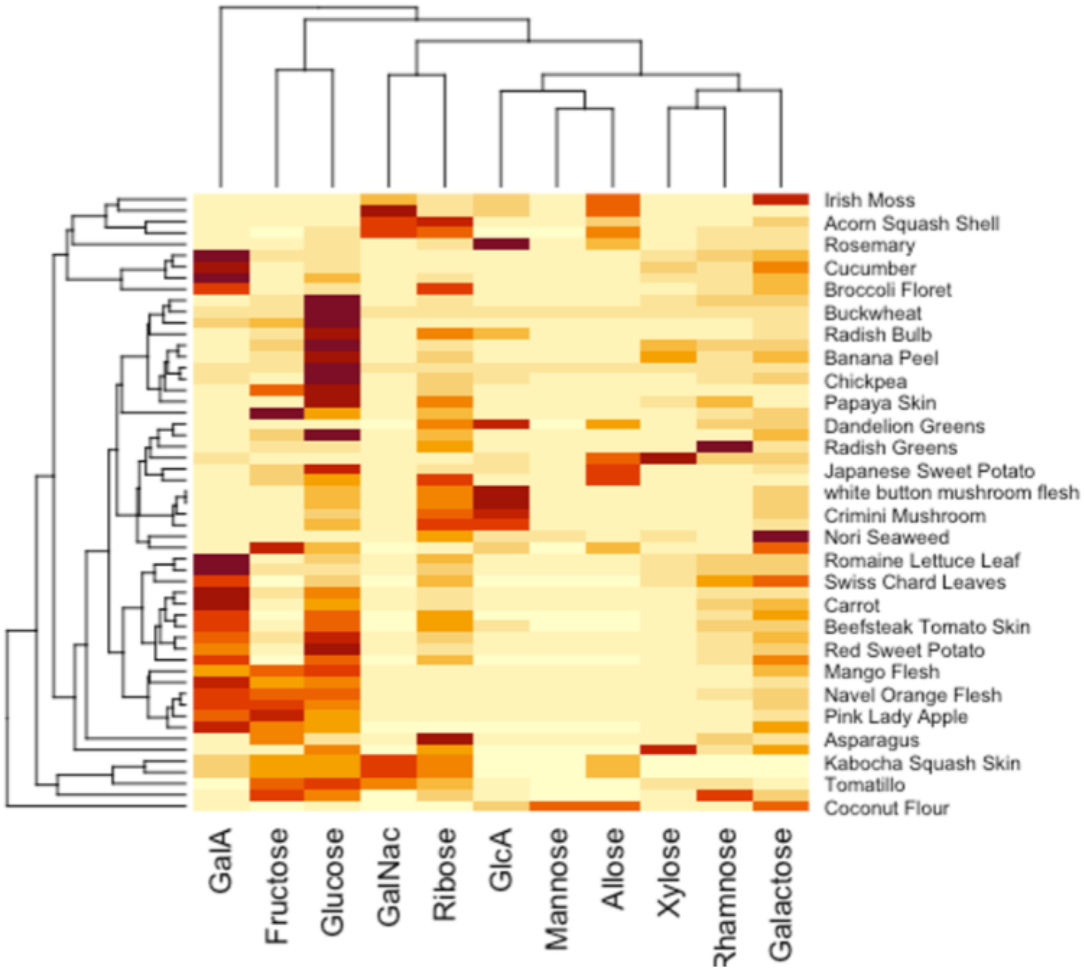

Figure 2.1. Hierarchical clustering of 55 fibers based on their absolute monosaccharide composition. Monosaccharide data were corrected by the input mass of each fiber and scaled by minimum and maximum values. Clustering analysis was performed with the hclust function in R. A maximum value of Dunn's index (0.648162) was obtained at k=43. Results similar for average and complete linkage.

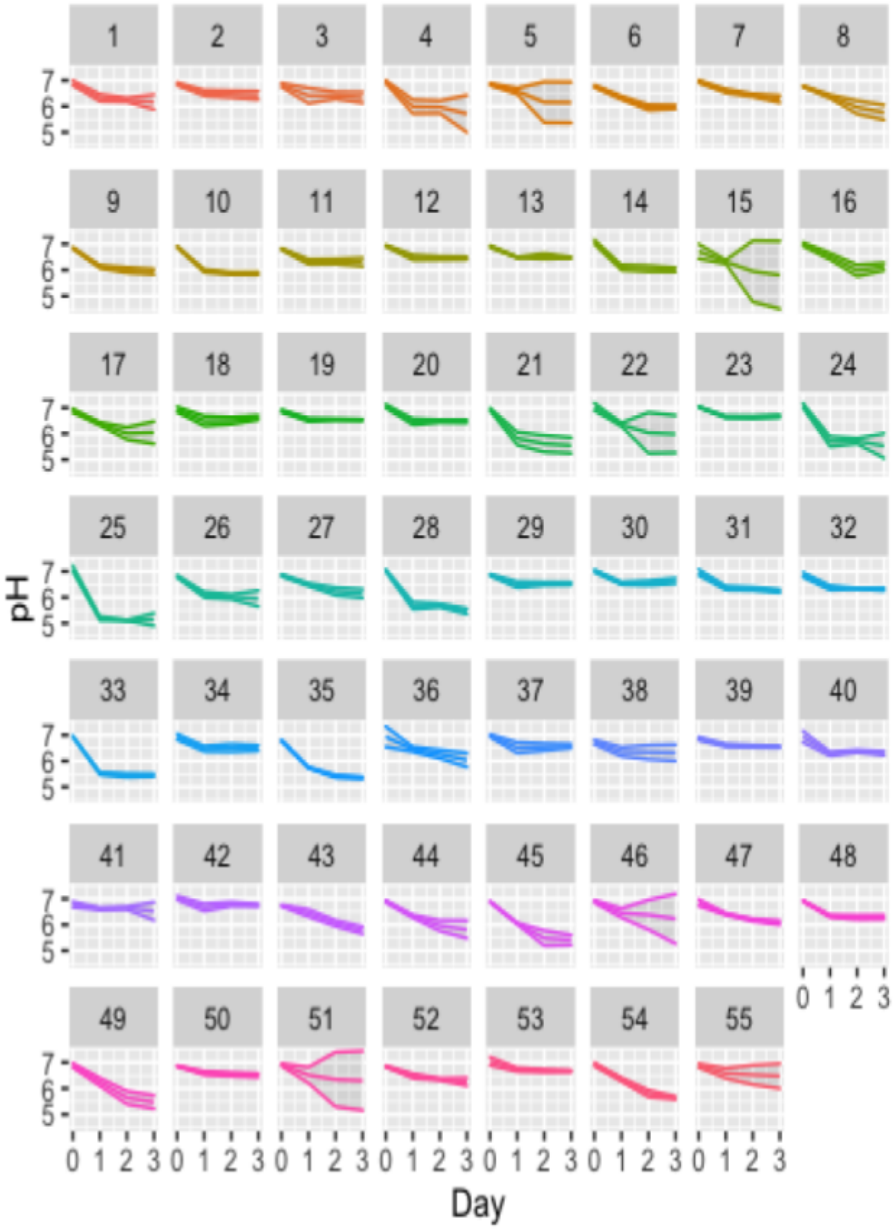

1. Acorn Squash Flesh
2. Acorn Squash Shell
3. Asparagus
4. Banana Fruit
5. Banana Peel
6. Beefsteak Tomato Flesh
7. Beefsteak Tomato Skin
8. Bok Choi
9. Broccoli Floret
10. Buckwheat
11. Carrot
12. Cashew
13. Celery Stalk
14. Chickpea
15. Coconut Flour
16. Crimini Mushroom
17. Cucumber
18. Dandelion Greens
19. Fingerling Potato Skin
20. Formosa Papaya Flesh
21. Garlic
22. Granny Smith Apple
23. Irish Moss
24. Japanese Sweet Potato
25. Kabocha Squash Flesh
26. Kabocha Squash Skin
27. Kale Leaves
28. Kidney Bean
29. Kiwi Flesh
30. Kiwi Skin
31. Mango Flesh
32. Mango Skin
33. Millet
34. Navel Orange Flesh
35. Navel Orange Peel
36. Nori Seaweed
37. Papaya Skin
38. Pink Lady Apple
39. Portobello Mushroom Flesh
40. Prune
41. Psyllium Husk
42. Radish Bulb
43. Radish Greens
44. Red Bell Pepper
45. Red Sweet Potato
46. Romaine Lettuce Leaf
47. Rosemary
48. Snap Pea Pods
49. Snow Pea Pods
50. Swiss Chard Leaves
51. Tomatillo
52. White Button Mushroom Flesh
53. White Button Mushroom Skin
54. White Onion Peel
55. Yellow Zucchini Squash

Figure 2.2. pH change over the course of 72-hour fermentations. pH was measured every 24 hours. Lines show mean +/- 2*standard deviation.

Variable	Transformation	Beta-coefficient	95% CI	p-value
Intercept	NA	6.469254	6.19613748—6.742371072	<2e-16
Glucose	Box-Cox	-0.021658	-0.04071189—-0.002603318	0.0267
Xylose	Box-Cox	0.125097	0.01999176—0.230201350	0.0206
Rhamnose	Box-Cox	-0.655681	-1.50876072—0.197399399	0.129

Table 2.1. Generalized linear model to predict final pH from fiber monosaccharide composition. The influence of each variable on final pH was assessed with purposeful selection modeling. Box-Cox transformations were applied to monosaccharide data due to deviations from normality. Rhamnose was included in the model as a confounder of xylose. Monosaccharide data were scaled by minimum and maximum values.

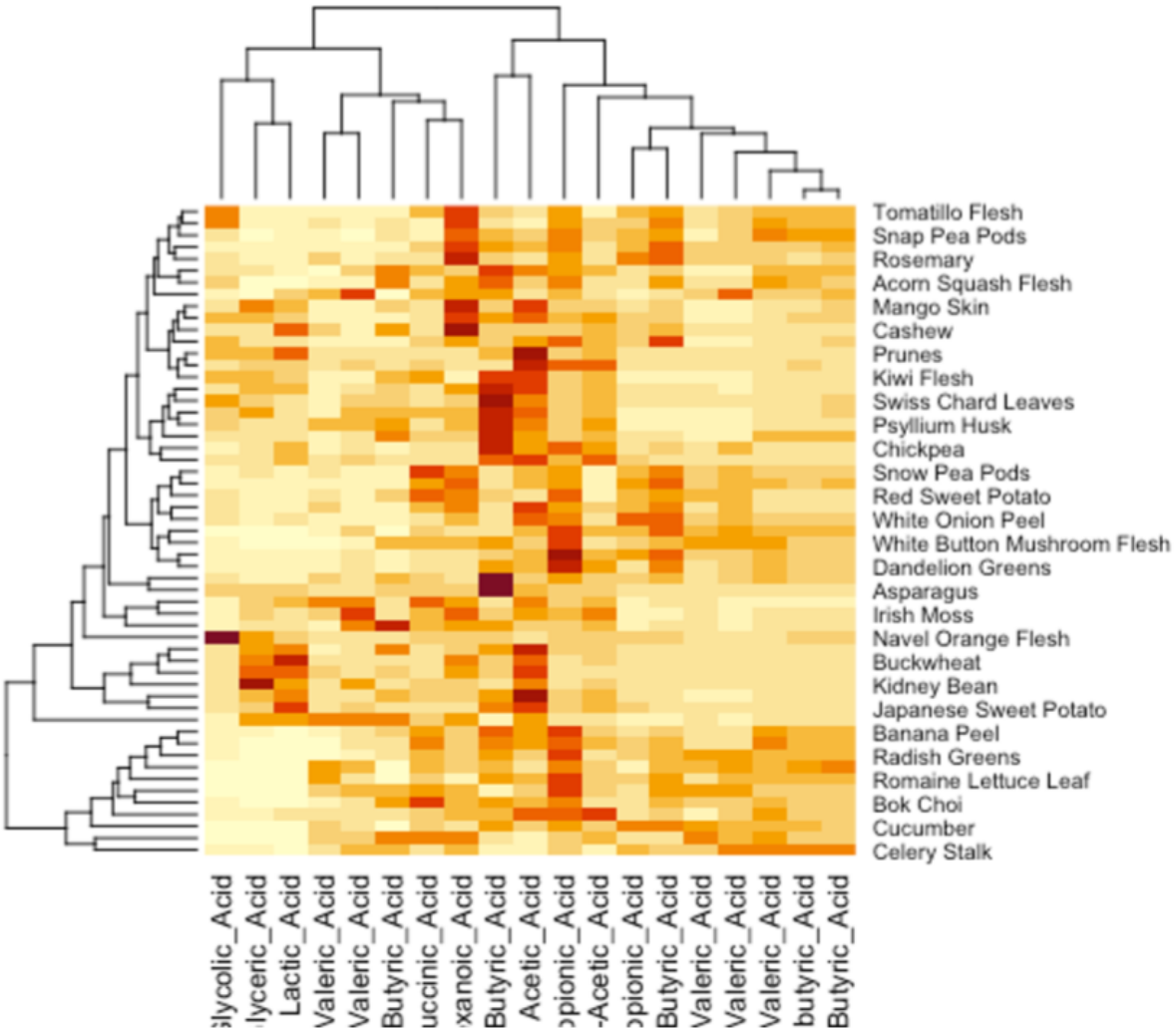

Figure 2.3. Hierarchical clustering of fibers based on post-fermentation acidic microbial metabolite levels. Average acidic microbial metabolite data were scaled by minimum and maximum values. Clustering analysis was performed with the hclust function in R. A maximum value of Dunn's index (0.762873) was obtained at 5=51. Results based on average and complete linkage were similar.

Variable	Transformation	Beta-coefficient	95% CI	p-value
Acetic Acid	log10	-1.03608	-1.33059054—-0.741563431	9.57E-11
Propionic Acid	Box-Cox	-0.42555	-0.56812336—-0.282979149	2.25E-08
Glyceric Acid	Box-Cox	0.14912	-0.29932019—0.001077643	0.0516
I3A	Box-Cox	-0.34931	0.26639344—0.432222381	4.20E-14
Glycolic Acid*	Box-Cox	0.02928	-0.03852156—0.097076418	0.395

Table 2.2. Generalized linear model to predict final pH from final acidic microbial metabolite levels. Unscaled 72-hour metabolite data were classified into tertiles. Log10 or Box-Cox transformations were applied to metabolite data due to deviations from normality. Glycolic acid was included in the model as a confounder of glyceric acid.

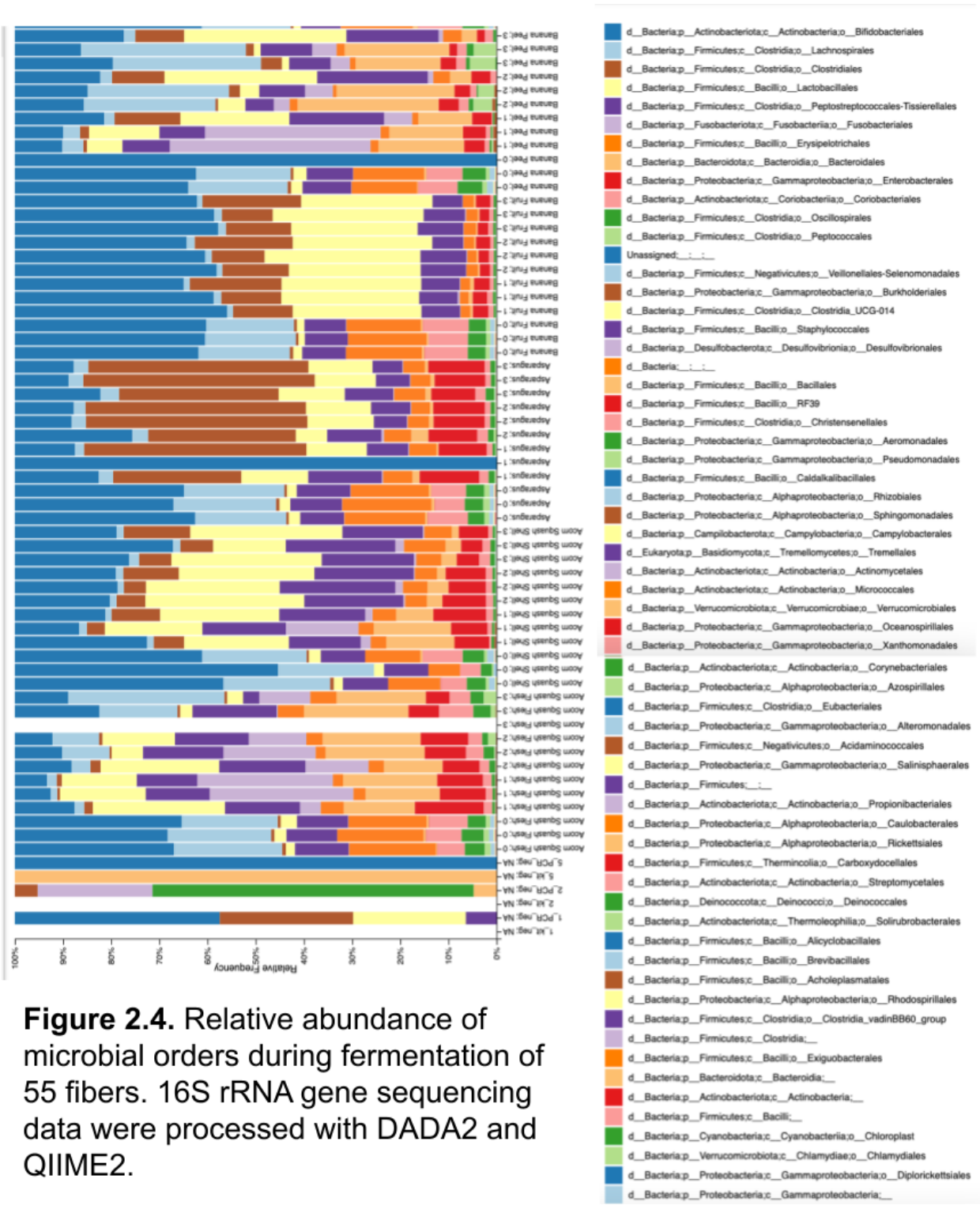

Figure 2.4. Relative abundance of microbial orders during fermentation of 55 fibers. 16S rRNA gene sequencing data were processed with DADA2 and QIIME2.

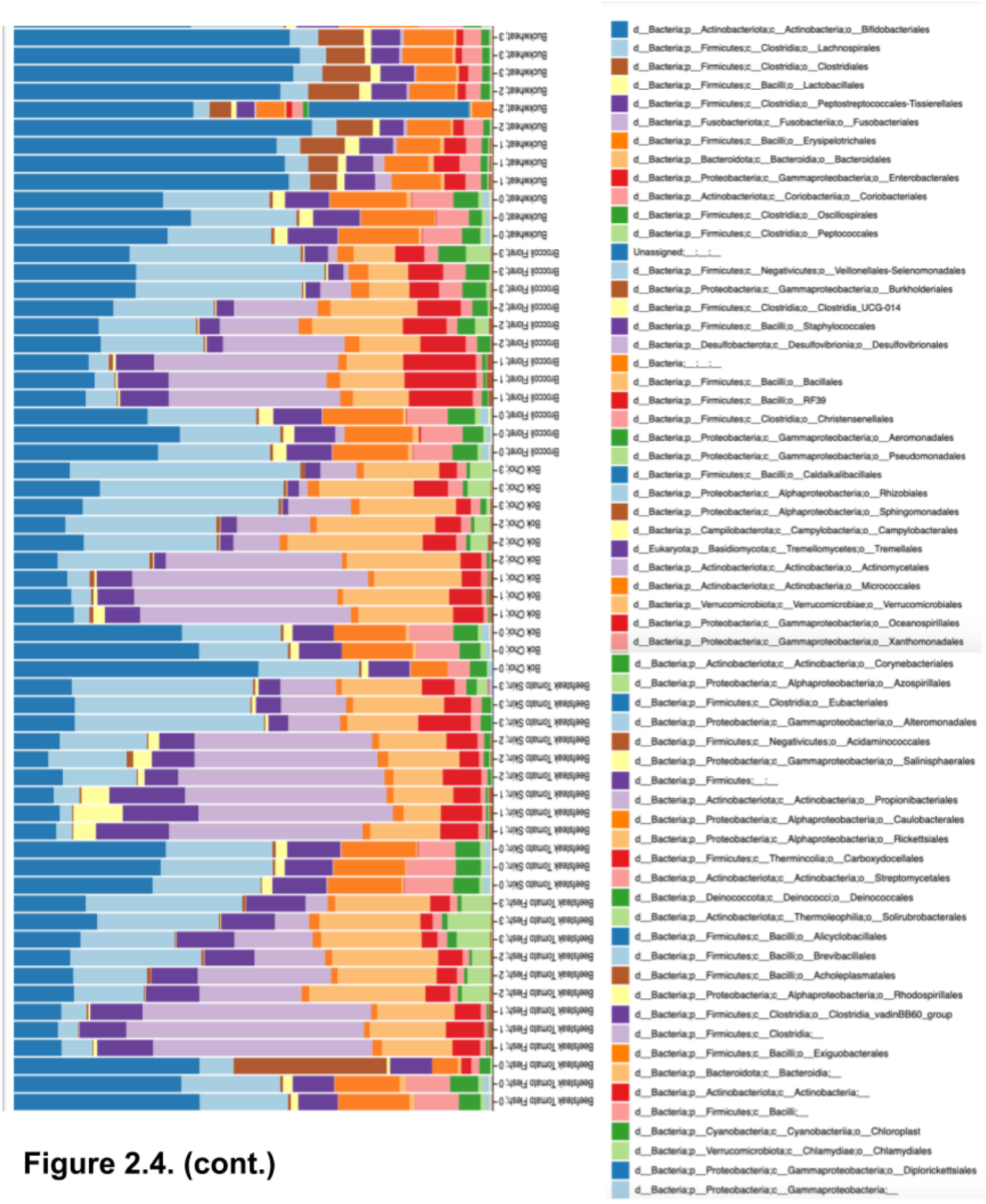

Figure 2.4. (cont.)

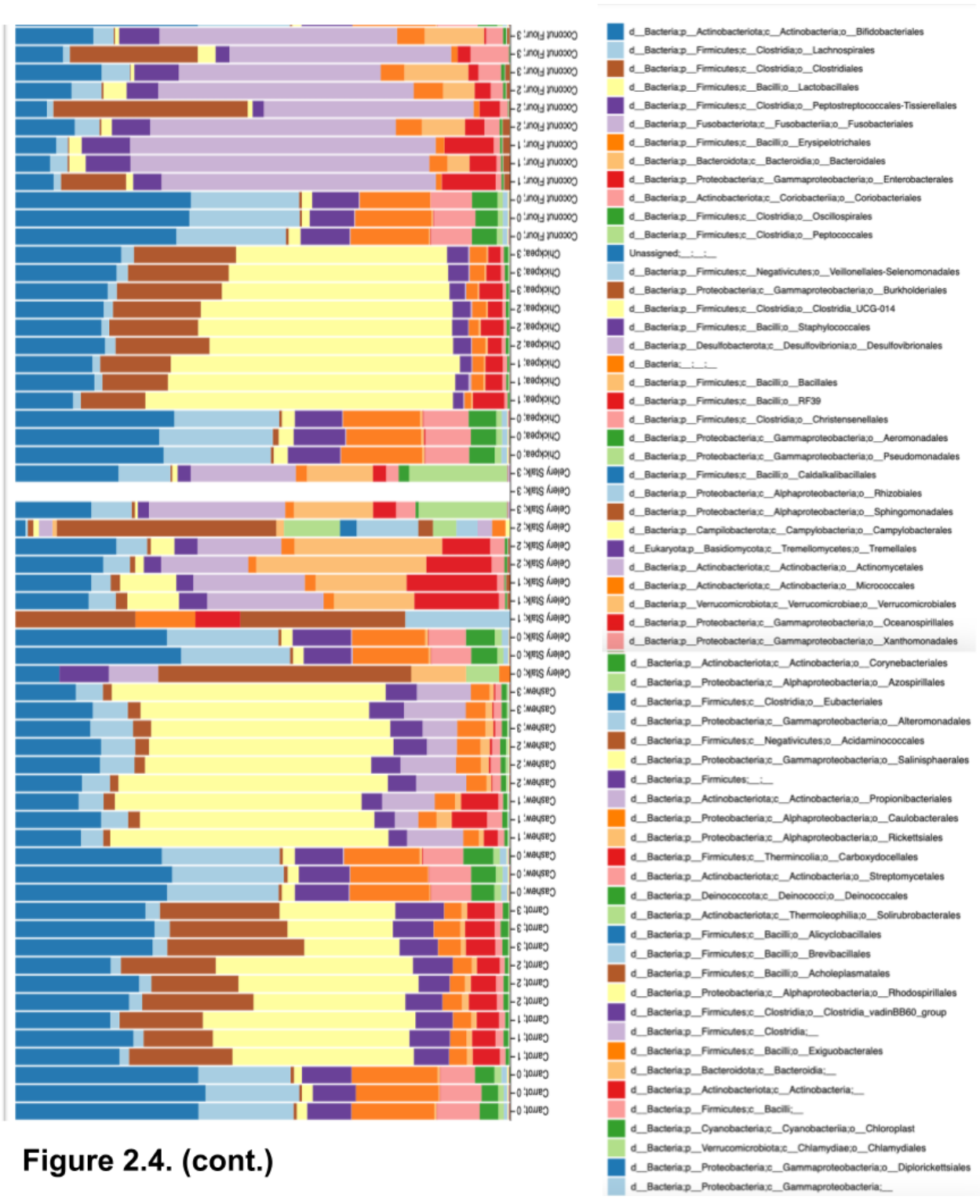

Figure 2.4. (cont.)

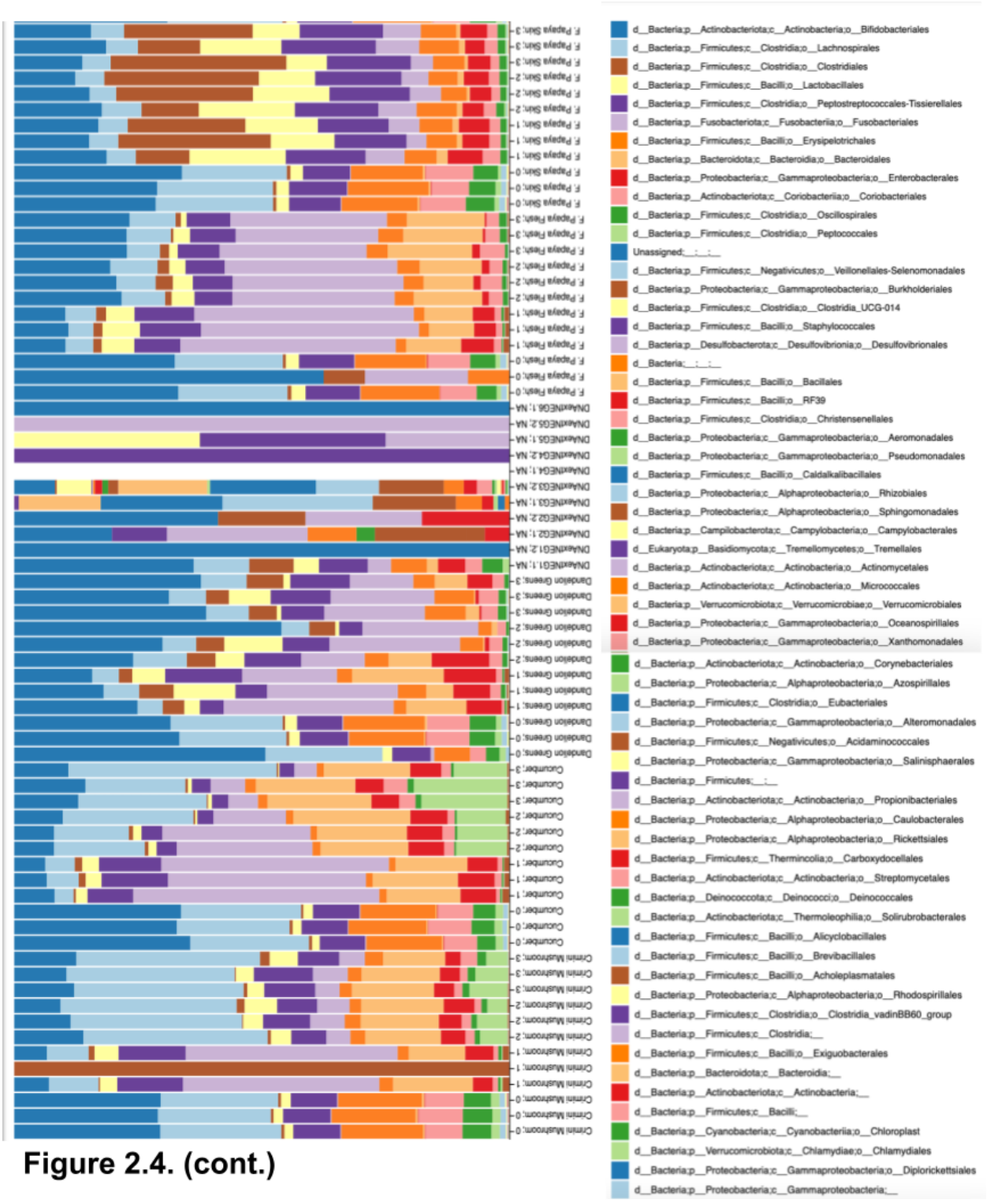

Figure 2.4. (cont.)

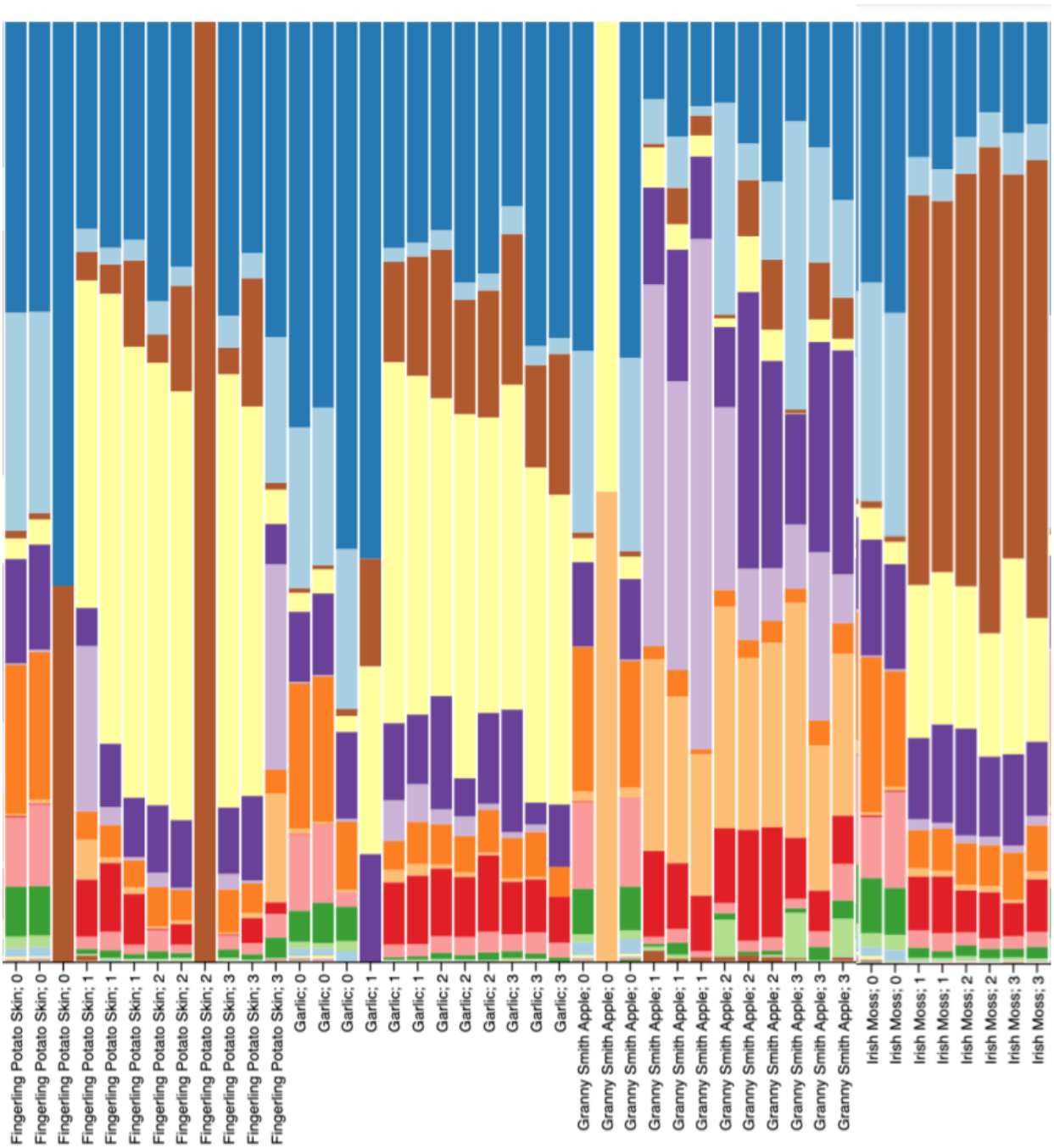

Figure 2.4. (cont.)

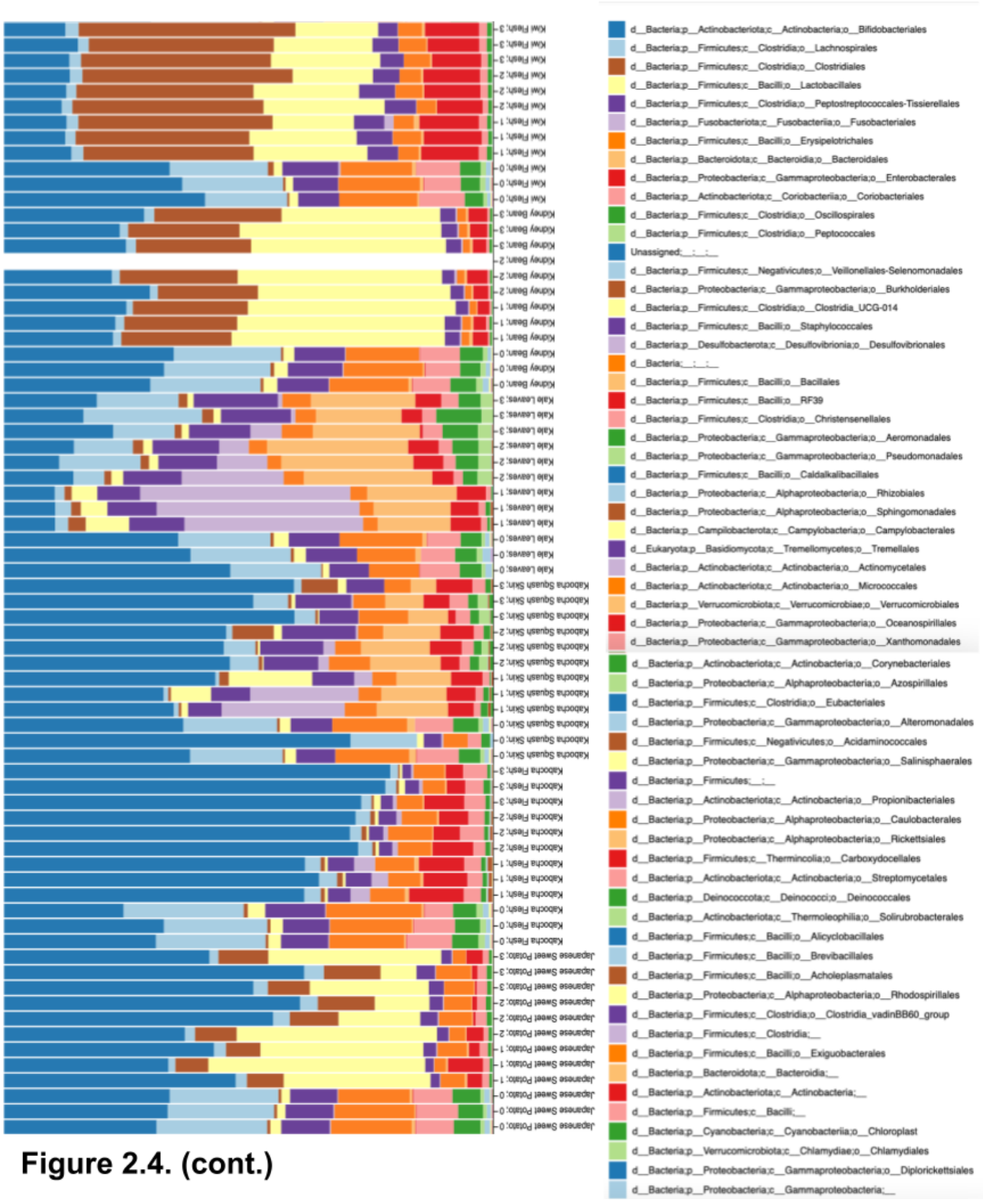

Figure 2.4. (cont.)

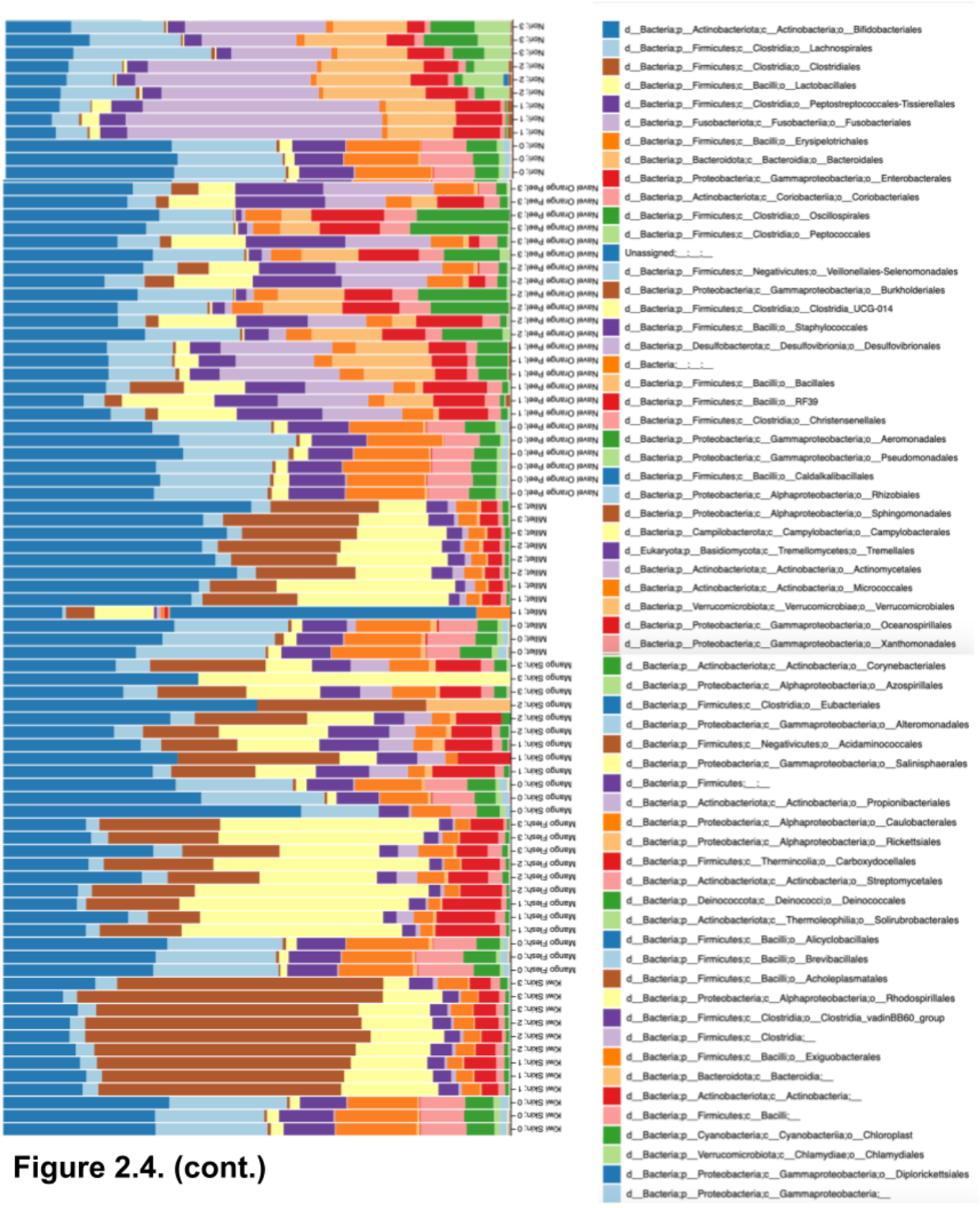

Figure 2.4. (cont.)

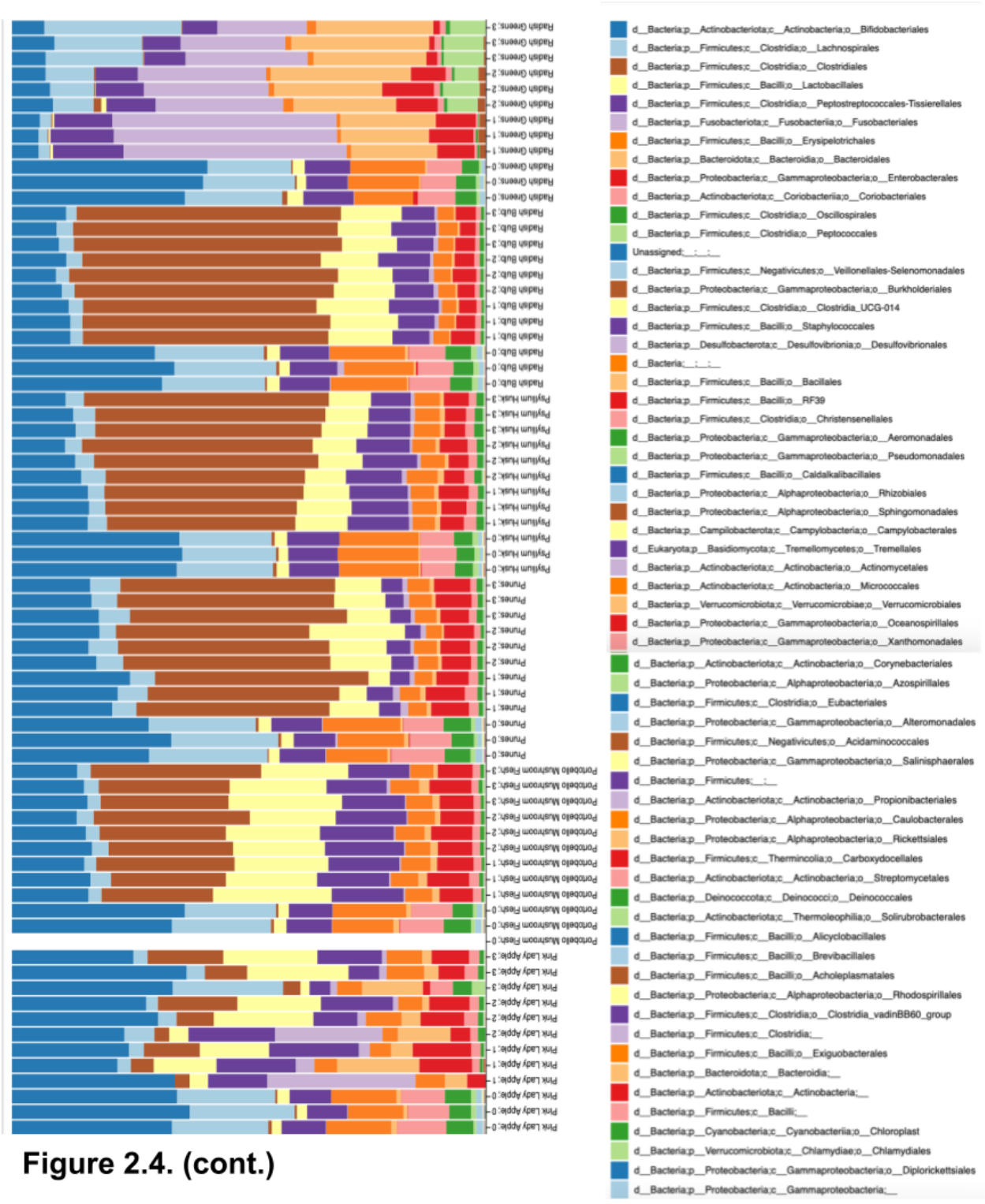

Figure 2.4. (cont.)

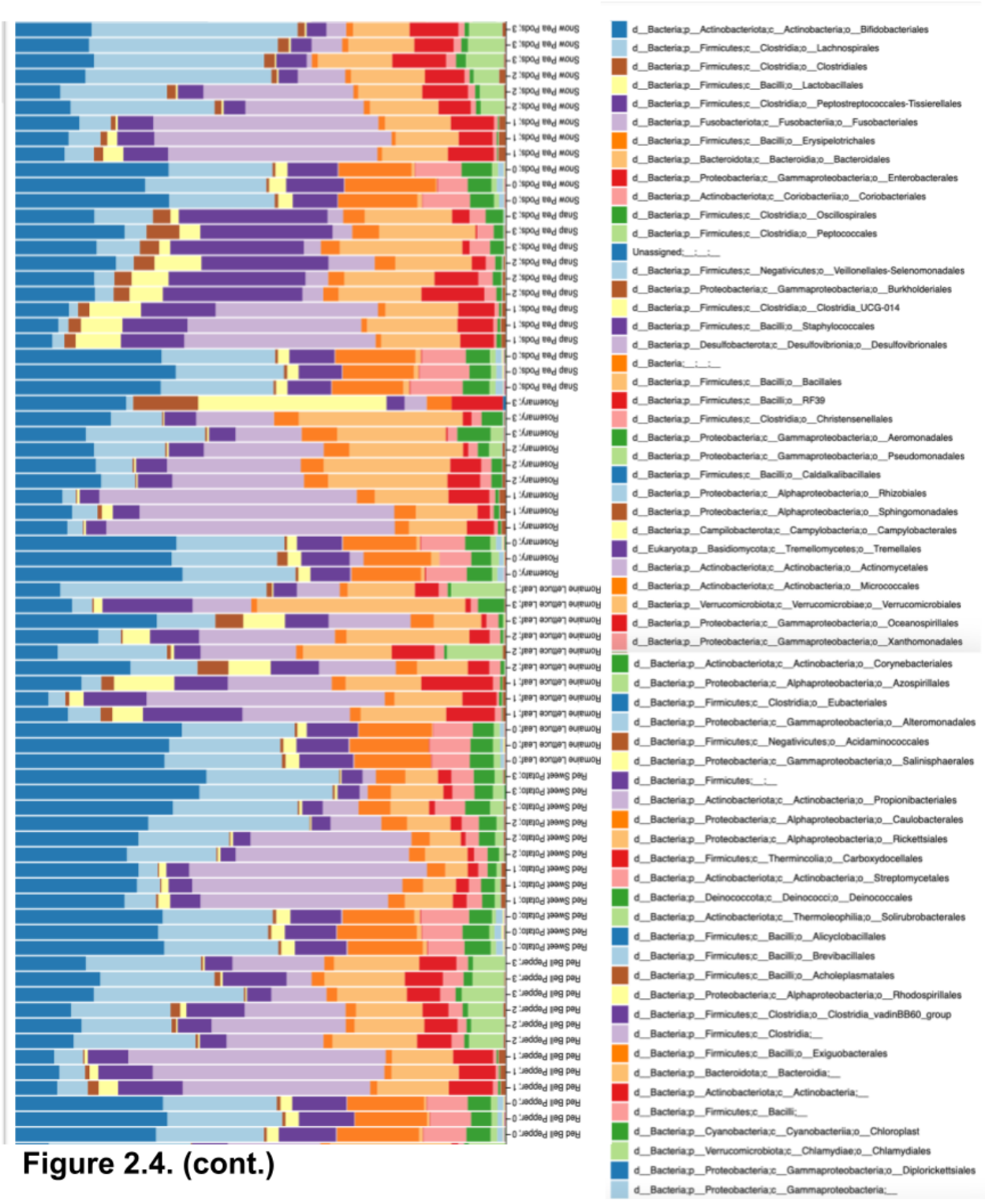

Figure 2.4. (cont.)

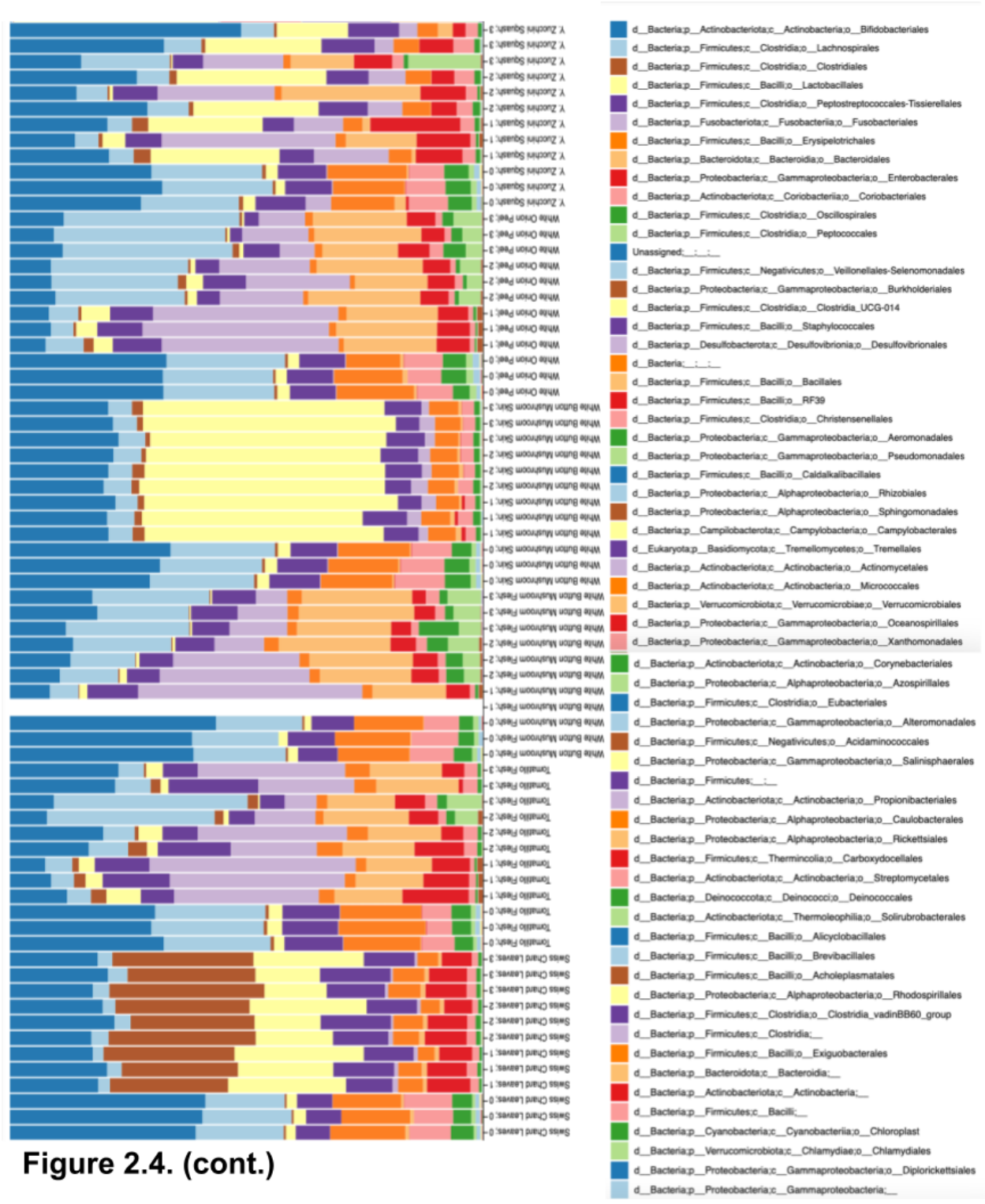

Figure 2.4. (cont.)

Variable	Estimate	95% CI	p-value
Intercept	2.18994	2.08957238—2.29044225	< 2e-16
Day	0.135764	0.10524662—0.16632594	< 2e-16
Xylose	-0.007075	-0.01271996—-0.00143233	0.0145
Rhamnose	0.149041	0.09409836—0.20393189	2.99E-07
GalA	0.039422	0.02377363—0.05505690	1.71E-06
GlcA	0.608678	0.09995681—1.11776534	0.0195

Table 2.3. Linear mixed effects model to predict longitudinal alpha diversity. The model included baseline alpha diversity and each monosaccharide as a fixed effect and bioreactor ID as a random effect. Modeling was performed with lme4. Monosaccharide data were normalized by scaling from 0-1.

Variable	p-value
Sequencing Run	0.003
Glucose	0.015
Galactose	0.033
Fructose	0.013
Rhamnose	0.004
GalA	0.001
GalNac	0.009
Mannose	0.001
Allose	0.016

Table 2.4. Day 3 PERMANOVA of microbiome data from 72-hour fermentation samples. PERMANOVA was performed with 999 permutations on a distance matrix of Bray–Curtis distances with the adonis2 function (vegan package). Rarefied 16S rRNA data (rarefaction depth=2509) were used due to >10-fold read differences between samples.

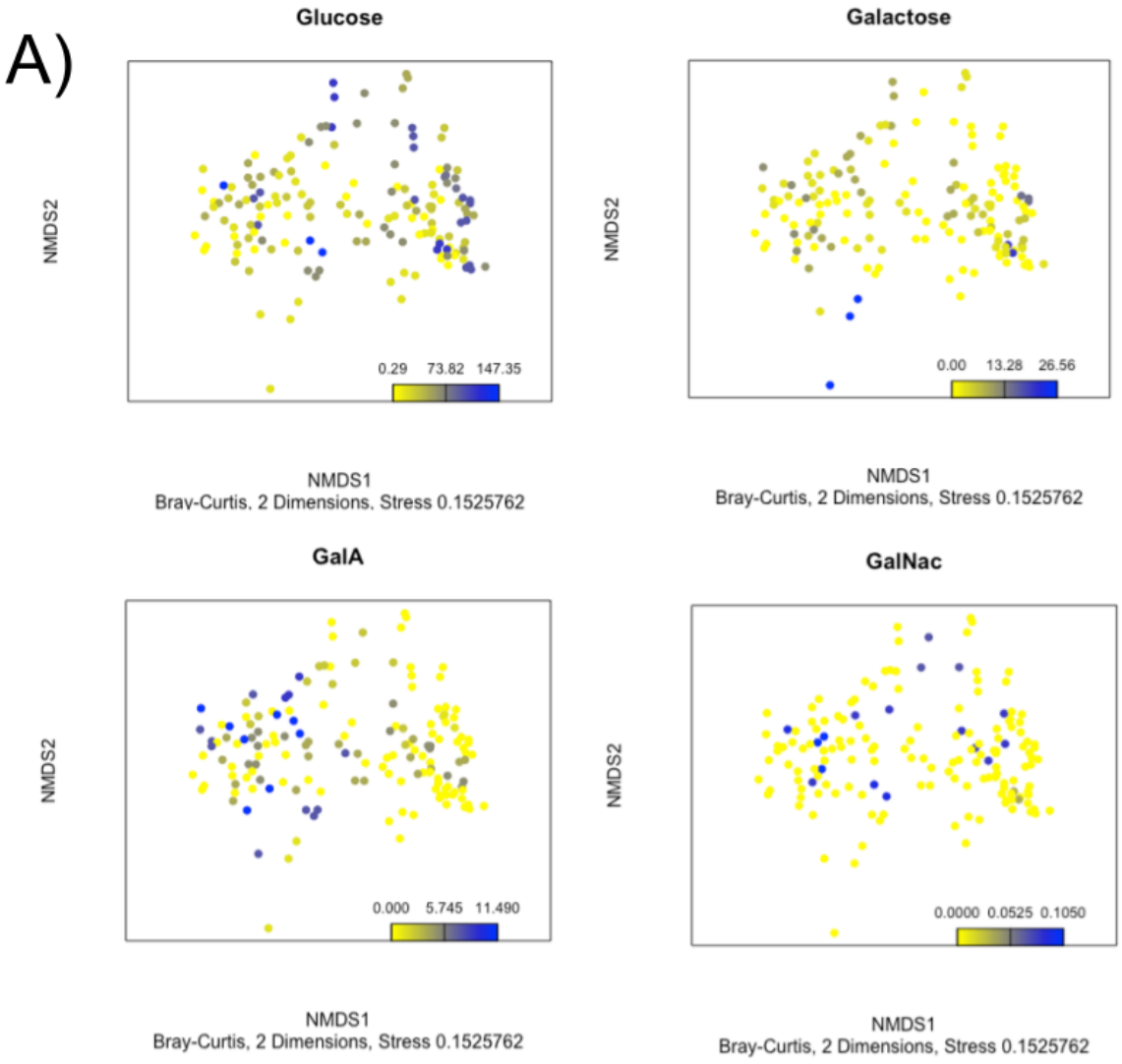

Figure 2.5. Gradient plots of microbiome samples after 72 hours of fermentation. Ordination was performed with non-metric multidimensional scaling (NMDS) of a distance matrix of Bray–Curtis distances. A) Monosaccharide content of food used in fermentation

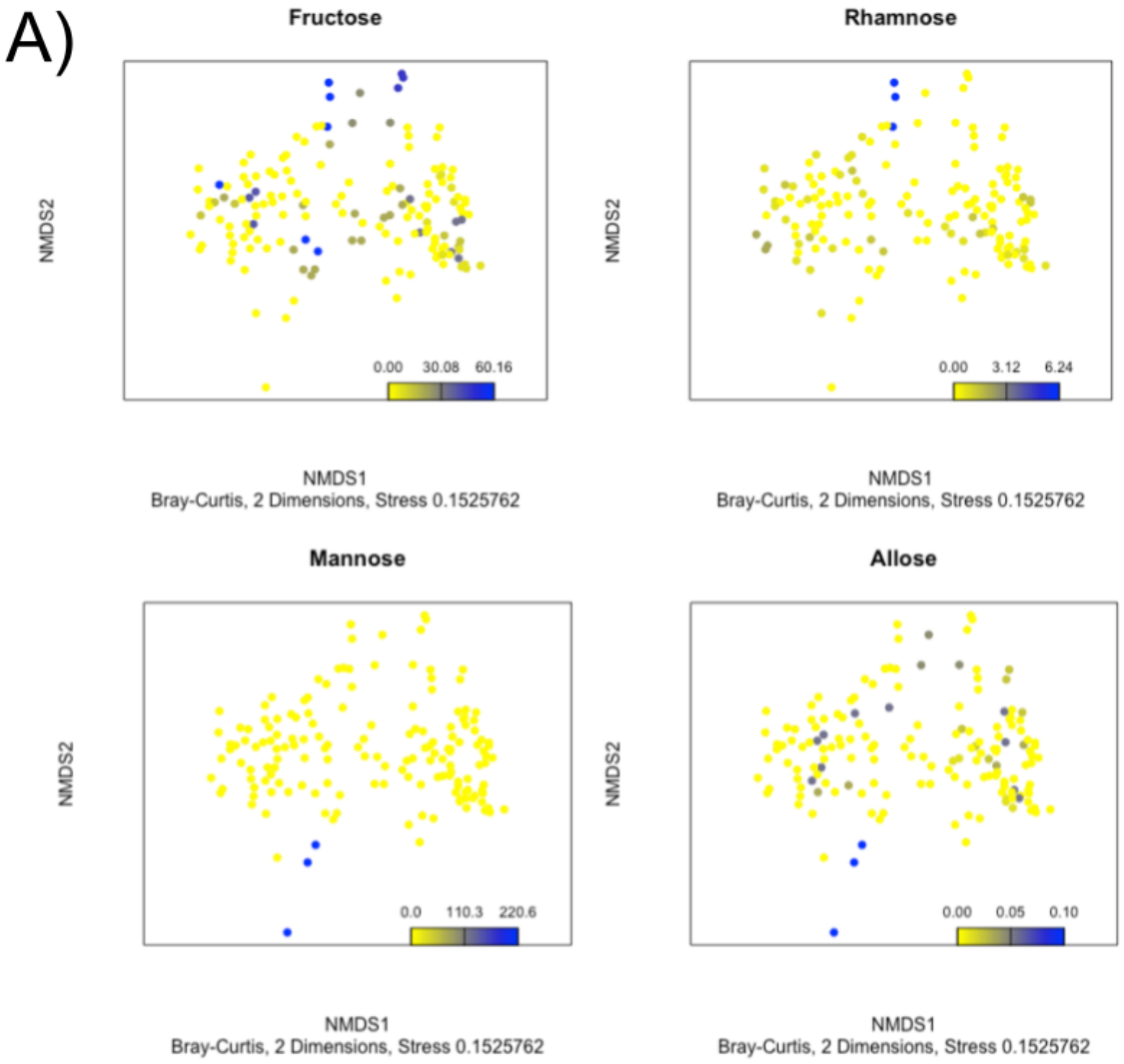

Figure 2.5. A) (cont.)

B)

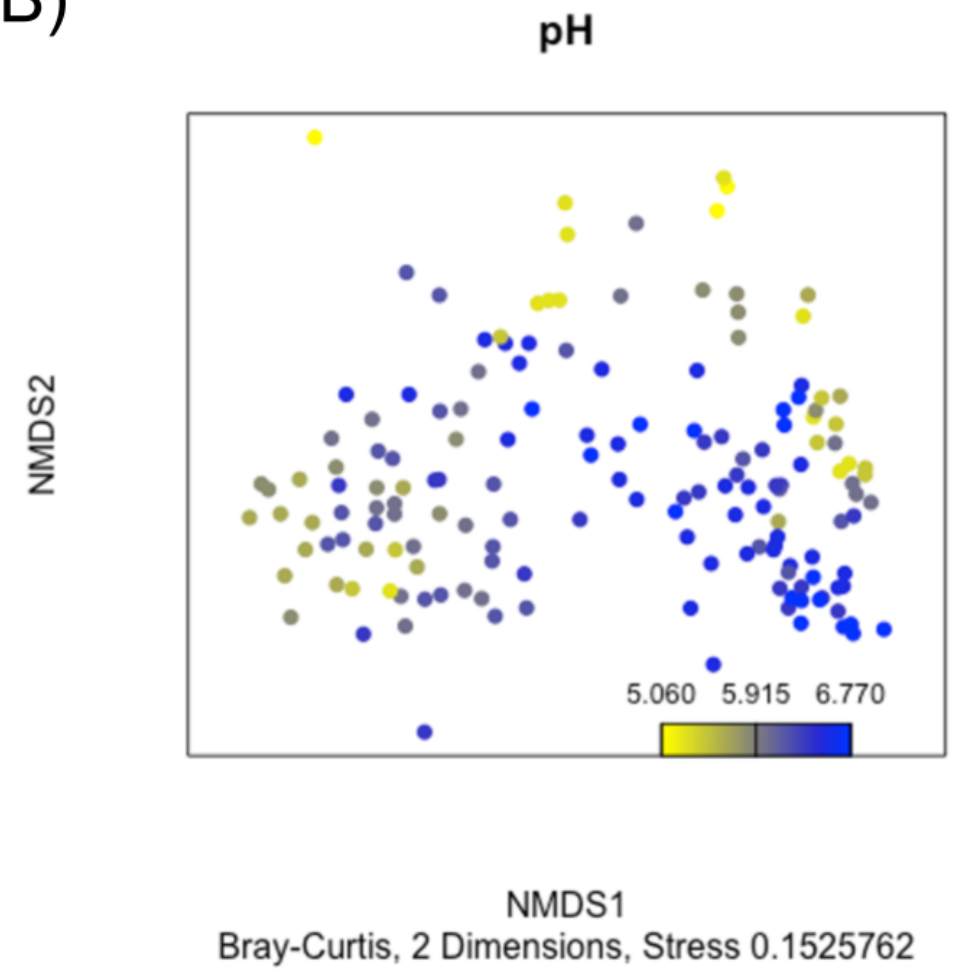

Figure 2.5. B) Final pH

Sugar	W-statistic	CLR mean difference	Genus
Allose	97	23.43	Dubosiella
Fructose	54	11.04	[Eubacterium] brachy group
GalA	81	9.65	Libanicoccus
GalA	73	8.35	Alistipes
GalA	71	9.72	Phocea
Galactose	73	10.83	UBA1819
GalNac	107	57.41	Dubosiella
GlcA	93	23.83	Dubosiella
Glucose	41	8.81	Holdemanella
Mannose	119	21.6	Clostridium sensu stricto 1
Rhamnose	108	9.54	Lactobacillus
Ribose	67	9.3	Flavonifractor
Xylose	118	12.06	Lachnospira

Table 2.5. Analysis of Compositions of Microbiomes (ANCOM) results for fiber monosaccharide data. 16S rRNA sequencing data taken after 72 hours of fermentation was tested for differential abundance based on fiber monosaccharide content. Monosaccharide data were classified into tertiles and sequencing data were analyzed at the genus level.

AMM	W-statistic	CLR mean difference	Genus
Acetic Acid	114	16.53	Escherichia-Shigella
Acetic Acid	107	9.55	Clostridium sensu stricto 1
2,2-DimethylButyric Acid	57	0.55	Dubosiella
Glyceric Acid	118	27.32	Clostridium sensu stricto 1
Glyceric Acid	118	23.01	Lactobacillus
Glyceric Acid	113	21.1	[Ruminococcus] torques group
Glyceric Acid	110	21.95	Unknown Lachnospiraceae genus
Glyceric Acid	108	15.6	Romboutsia
Glyceric Acid	104	20.12	Fusobacterium
Glyceric Acid	104	18.72	Bacteroides
Glyceric Acid	102	17.59	Colidextribacter
Glyceric Acid	101	12.53	Lachnospira
Glyceric Acid	99	14.48	Coprococcus
Glycolic Acid	30	7.7	Dubosiella
Glycolic Acid	12	7.28	[Eubacterium] brachy group
Glycolic Acid	10	4.54	Libanicoccus
Glycolic Acid	9	7.34	Blautia

Table 2.6. ANCOM results for acidic microbial metabolites (AMMs) 16S rRNA sequencing data taken after 72 hours of fermentation was tested for differential abundance based on tertiles of each AMM in the corresponding fermenter. Sequencing data were analyzed at the genus level.

AMM	W-statistic	CLR mean difference	Genus
Glycolic Acid	7	3.55	Parabacteroides
Indole-3-Acetic Acid	44	11.01	Mogibacterium
Indole-3-Acetic Acid	39	10.23	Collinsella
Indole-3-Propionic Acid	118	39.19	Lactobacillus
Indole-3-Propionic Acid	118	40.56	Clostridium sensu stricto 1
Indole-3-Propionic Acid	116	40.16	Romboutsia
Indole-3-Propionic Acid	114	31.43	[Ruminococcus] torques group
Indole-3-Propionic Acid	113	53.79	Unknown Lachnospiraceae genus
Indole-3-Propionic Acid	113	32.83	Colidextribacter
Indole-3-Propionic Acid	112	35.49	Alistipes
Indole-3-Propionic Acid	111	38.65	Bacteroides
Indole-3-Propionic Acid	110	22.92	Peptococcus
Indole-3-Propionic Acid	107	19.41	Enterococcus
Indole-3-Propionic Acid	106	25.56	[Ruminococcus] gauvreauii group
Indole-3-Propionic Acid	105	29.45	RF39
Indole-3-Propionic Acid	104	24.31	Solobacterium
Indole-3-Propionic Acid	103	24.67	Coprococcus

Table 2.6. (cont.)

AMM	W-statistic	CLR mean difference	Genus
Indole-3-Propionic Acid	98	20.14	Oscillibacter
Indole-3-Propionic Acid	97	22.47	Dialister
Indole-3-Propionic Acid	97	21.06	Libanicoccus
Indole-3-Propionic Acid	96	20.44	Butyricimonas
Indole-3-Propionic Acid	96	14.61	Odoribacter
Indole-3-Propionic Acid	95	13.16	Lachnospira
Indole-3-Propionic Acid	94	14.31	Sutterella
Indole-3-Propionic Acid	94	10.64	Parabacteroides
Indole-3-Propionic Acid	94	14.83	Negativibacillus
Indole-3-Propionic Acid	94	18.17	Clostridia UCG-014
Indole-3-Propionic Acid	93	13.15	Uncultured Desulfovibrionaceae
Indole-3-Propionic Acid	91	13.65	Fusobacterium
Indole-3-Propionic Acid	90	10.16	Phocea
Indole-3-Propionic Acid	90	9.55	Uncultured Lachnospiraceae
Propionic Acid	118	55.24	Clostridium sensu stricto 1
Propionic Acid	118	65.31	Lactobacillus
Propionic Acid	117	45.88	Romboutsia

Table 2.6. (cont.)

AMM	W-statistic	CLR mean difference	Genus
Propionic Acid	113	34.57	[Ruminococcus] torques group
Propionic Acid	113	46.34	Alistipes
Propionic Acid	112	51.11	Colidextribacter
Propionic Acid	111	41.14	Unknown Lachnospiraceae
Propionic Acid	110	39.72	Bacteroides
Propionic Acid	108	33.34	Peptococcus
Propionic Acid	108	29.98	Solobacterium
Propionic Acid	107	33.49	[Ruminococcus] gauvreauii group
Propionic Acid	105	31.29	Coprococcus
Propionic Acid	104	28.64	RF39
Propionic Acid	101	28.14	Dialister
Propionic Acid	100	20.19	Lachnospira
Propionic Acid	99	23.85	Butyricimonas
Propionic Acid	99	27.48	Oscillibacter
Propionic Acid	99	23.47	Libanicoccus
Propionic Acid	98	23.88	Negativibacillus
Propionic Acid	97	16.34	Enterococcus

Table 2.6. (cont.)

Supplementary Figures and Tables

	SSF			SGF			SIF		
Constituent	Min mmol $^{-1}$	Max mmol $^{-1}$	Reference	Min mmol $^{-1}$	Max mmol $^{-1}$	Reference	Min mmol $^{-1}$	Max mmol $^{-1}$	Reference
Cl^-	16.8	36	(Altman 1968)	156	166	(Altman 1968)	67	93	(Altman 1968)
K^+	7.7	9.2	(Altman 1968)	12	14	(Altman 1968)	3.5	4.1	(Case et al. 1969)
Na^+	24	46	(Altman 1968)	12	56	(Altman 1968)	156.5	159.5	(Case et al. 1969)
HCO_3-, CO_3^{2-}	11.6	13.6	(Altman 1968)	--	--	--	139	145	(Case et al. 1969)
Ca^{2+}	--	--	--	1	2.5	(Altman 1968)	2.3	2.55	(Altman 1968)
$H_2PO_4^-$	--	--	--	0.06	0.19	(Altman 1968)	--	--	--
NH_4^+	--	--	--	7.1	29.3	(Altman 1968)	--	--	--

Table S2.1. Reference ranges of mineral concentrations used to prepare simulated digestive fluids. SSF = simulated salivary fluids, SGF = simulated gastric fluids (SGF), SIF = simulated intestinal fluids.

			1.25x SSF		1.25x SGF		1.25x SIF	
			pH 7.5		pH 2.5 (Brosey et al., 2009)		pH 6.0 (Brosey et al., 2009)	
Constituent	Stock conc.		Vol. of stock	Conc. in SSF	Vol. of stock	Conc.. in SGF	Vol. of stock	Conc. in SIF
	mol L^{-1}	**g L^{-1}**	**mL**	**mmol L^{-1}**	**mL**	**mmol L^{-1}**	**mL**	**mmol L^{-1}**
KCl	0.5	37.3	8.5	8.5	12.9	12.9	3.8	3.8
KH_2PO_4	0.6	100.0			0.1	0.1		
$NaHCO_3$	1.0	84.0	6.0	12.0			67.6	135.2
Na_2CO_3	0.9	100.0	0.3	0.6			3.6	6.8
NaCl	2.0	116.9	5.5	21.8	8.5	34.0	4.0	16.0
$(NH_4)_2CO_3$	0.5	48.0			18.2	18.2		
$CaCl_2(H_2O)_2$**	0.3	44.1			2.9	1.8	4.0	2.4
** added $CaCl_2(H_2O)_2$ to final digestion mixture to avoid precipitation.								

Table S2.2. Final concentrations of simulated digestive fluids used in fecal fermentations. SSF = simulated salivary fluids, SGF = simulated gastric fluids (SGF), SIF = simulated intestinal fluids. Concentrations in simulated fluids were averages of the mineral concentrations listed.

Fiber Source	Glucose	Galactose	Fructose	Xylose	Arabinose	Fucose	Rhamnose	GlcA	GalA	GlcNac	GalNac	Mannose	Allose	Ribose
Acorn Squash Flesh	0.23555211	0.04217332	0.01261574	0.06600061	0.03172501	0.0051869	0.01057239	0.0001710 1	0.00699208	0.0004982	0.0004945 9	0.00943945	0.0003877 6	0.0071699 6
Acorn Squash Shell	0.04643807	0.04499399	0.03077143	0.01093695	0.03682604	0.0036635 6	0.00223351	0	0.00029855	0.0005048 6	0.0005014	0.00152412	0.0001498 4	0.0087490 1
Asparagus	0.07051704	0.00710203	0.15024224	0.00986876	0.01958845	0.0027187	0.00501848	2.42E-05	0.00027351	0.0007848 6	0	0.00335942	0	0.0075184
Banana Fruit	0.587824	0.005101	0.076219	0.001678	0.002785	0.000512	0.000127	0	0.010255	0	0	0.003338	0	0
Banana Peel	0.28235254	0.01646981	0.01905177	0.05382445	0.09409066	0.0054627 9	0.00218297	0	8.69E-05	2.11E-05	0	0.00160683	0	0.0009116 3
Beefsteak Tomato Flesh	0.46860847	0.01267205	0.18114897	0.01306205	0.01899999	0.0008147 6	0.00267903	0.0001057 8	0.02214341	0.0004903 9	0.0004921 3	0.005695	0.0002624 5	0.0061745 8
Beefsteak Tomato Skin	0.25398988	0.01647124	0.00814139	0.01276 17	0.01179251	0.0004834 6	0.0043179	0.0003391	0.02326807	0.0002008	0	0.00546703	0	0.0018438 5
Bok Choi	0.098522	0.020632	0.01934	0.0196	0.011498	0.003232	5	0	0.051259	0	0	0.003444	0	0.00153
Broccoli Floret	0.090832	0.031702	0	0.015169	0.03592	0.0035622	0.00394	0	0.030295	0	0	0.005937	0	0.0042 01
Buckwheat	0.596802	0.008478	0.003687	0.001338	0.012071	0.000397	0.000521	0.0000507	0.000793	0	0	0.000462	0	0.0005 39
Carrot	0.216091	0.029694	0.002821	0.00759	0.023397	0.00234	0.003902	0	0.035386	0	0	0.004069	0	0.0008 11
Cashew	0.118189	0.007607	0.008233	0.00109	0.006731	0.000437	0.000195	0	0.000386	0	0	0.000254	0	0.0004 21
Celery Stalk	0.136339	0.031817	0	0.020124	0.023119	0.0036933	0.003358	0	0.038257	0	0	0.006365	0	0.0007 77
Chickpea	0.391161	0.012416	0.002855	0.002187	0.050521	0.000735	0.000768	0.000138	0.001359	0	0	0.000773	0	0.0005 99

Table S2.3. Unadjusted absolute monosaccharide composition of food fibers used in this study. Data reported as mg monosaccharide per mg of dry fiber.

Fiber Source	Glucose	Galactose	Fructose	Xylose	Arabinose	Fucose	Rhamnose	GlcA	GalA	GlcNac	GalNac	Mannose	Allose	Ribose
Coconut Flour	0.055003	0.053115	0	0.017178	0.014348	0	0.001241	0.000492	0.003273	0	0	0.441203	0.000194	0
Crimini Mushroom	0.084981	0.010983	0	0.008873	0.001533	0.00222	0.000209	0.00116	0	0	0	0.00613	0	0.00237
Cucumber	0.062325	0.04365	0	0.033184	0.010879	0.005453	0.00287	0	0.037654	0	0	0.009675	0	0
Dandelion Greens	0.01199271	0.00504599	0.00149698	0.00294383	0.00355206	0.00269857	0.00111693	0.00034746	0.00044253	8.82E-06	0	0.00059653	3.04E-05	0.00067602
Fingerling Potato Skin	0.00326818	0.00077376	0.00218886	0.001134 2	0.00102168	0.00061285	0.00034434	0.00059869	0.00050777	4.42E-05	0.00055358	0.00034687	0.00036479	0.00067559
Formosa Papaya Flesh	0.312956	0.008764	0.100901	0.007044	0.002751	0.001547	0.001345	0	0.036597	0	0	0	0	0
Garlic	0.21059142	0	0.0445902	0.00374434	0.02376513	0.00441954	0.00151607	1.01E-05	6.53E-05	3.28E-05	0	0.00069831	0.00020417	0.00336352
Granny Smith Apple	0.220683	0.015297	0.110965	0.015883	0.013303	0.003743	0.001238	0	0.021565	0	0	0.002496	0	0
Irish Moss	0.01625661	0.10280724	0.00516671	0.00242913	0.00033772	0.00201506	0.00063584	0.00054898	0.00020256	8.18E-05	0.0001746	0.00053629	0.00026124	0.00060301
Japanese Sweet Potato	0.232669	0.00595714	0.02355793	0.00147623	0.00364482	0.00025423	0.00048797	0.00013997	0.00022088	0	0	0.00017446	0.00014682	0.0004451
Kabocha Squash Flesh	0.17863119	0.017695	0.17548813	0.00139532	0.0069158	0.00055382	0.00110093	0	0.00019207	0	0	0.0012608	0	0.00130489
Kabocha Squash Skin	0.46860847	0.01267205	0.18114897	0.01306205	0.01899999	0.00081476	0.00267903	0.00010578	0.02214341	0.00049039	0.00049213	0.005695	0.00026245	0.00617458
Kale Leaves	0.119421	0.060376	0.02165	0.054851	0.056548	0.008625	0.007492	0	0.076576	0	0	0.017576	0	0
Kidney Bean	0.19460589	0.02732736	0.0038949	0.1249911	0.34136754	0.03073721	0.00284485	0	0.00010829	6.26E-05	0	0.00124991	0	0.00156976

Table S2.3. (cont.)

Fiber Source	Glucose	Galactose	Fructose	Xylose	Arabinose	Fucose	Rhamnose	GlcA	GalA	GlcNac	GalNac	Mannose	Allose	Ribose
Kiwi Flesh	0.236395	0.040807	0.116707	0.020297	0.008276	0.001836	0.00206	0	0.031804	0	0	0.003314	0	0
Kiwi Skin	0.42020664	0.01896429	0.04114054	0.06361536	0.03388066	0.00467145	0.00421933	0	8.62E-05	1.81E-05	0	0.0008259	0	0.00069671
Mango Flesh	0.476902	0.041161	0.167722	0.011355	0.028631	0.004838	0.001859	0	0.020906	0	0	0.004454	0	0
Mango Skin	0.15360109	0.05359293	0.14661233	0.00639967	0.03427026	0.00224569	0.00192991	0.00038833	0.00086065	0	0	0.00059729	9.08E-05	0.00028982
Millet	0.426439	0.002969	0.002723	0.001652	0.006473	0.000467	0.000082	0.0000733	0.000102	0	0	0.000194	0	0.000324
Navel Orange Flesh	0.303144	0.017473	0.125565	0.005637	0.011478	0.001831	0.002999	0	0.028455	0	0	0	0	0
Navel Orange Peel	0.18662048	0.01457813	0.10026764	0.00440032	0.07761232	0.00310618	0.01040164	4.30E-05	0.00043032	0	0	0.00315536	0	0.00094322
Nori Seaweed	0.001938	0.076812	0.000633	0.003182	0.000149	0.000683	0	5.75E-05	0	0.00E+00	0.00E+00	0.007537	0.00E+00	0.001787
Papaya Skin	0.42563676	0	0.00929626	0.01618435	0.01987286	0.00531474	0.00708998	6.41E-05	0.00078005	4.16E-05	0	0.00261996	0	0.00270606
Pink Lady Apple	0.171948	0.010501	0.133245	0.009041	0.015348	0.002918	0.001144	0	0.018813	0	0	0.001941	0	0
Portobello Mushroom Flesh	0.136565	0.012222	0	0.007204	0.001168	0.00203	0.000118	0.001447	0	0	0	0.009741	0	0.003769
Prune	0.75352145	0.02205308	0.02856127	0.01180131	0.0616266	0.00509593	0.00385984	0	0.00031765	1.8718E-05	0	0.00346495	0	0.00058505
Psyllium Husk	0.0047398	0.01111837	0.00154816	0.11846802	0.0484614	5.94E-05	0.00243689	0.00011129	0.00229453	0	0	0.00041484	0.00012726	0.00023431

Table S2.3. (cont.)

Fiber Source	Glucose	Galactose	Fructose	Xylose	Arabinose	Fucose	Rhamnose	GlcA	GalA	GlcNac	GalNac	Mannose	Allose	Ribose
Radish Bulb	0.61497764	0.01643033	0.04061288	0.00477626	0.03842467	0.00274726	0.00164626	0.0009715	0.00025481	0.00011458	0	0.00206837	0	0.0037671
Radish Greens	0.01101259	0.00337152	0.00206583	0.00130688	0.00528843	0.00279181	0.006773356	0	0	0	0	0.00016985	0	0.00076344
Red Bell Pepper	0.217437	0.005655	0.007207	0.001775	0.003111	0.004278	0.002474	0	0.03155	0	0	0	0	0.000238
Red Sweet Potato	0.484315	0.023677	0.008127	0.014089	0.012367	0.001245	0.002793	0	0.022417	0	0	0.000264	0	0.000469
Romaine Lettuce Leaf	0.118397	0.020955	0	0.025164	0.008702	0.00455	0.003707	0	0.034567	0	0	0.004576	0	0.001808
Rosemary	0.02099225	0.00870489	0.00148378	0.00127633	0.00566	0.00027543	0.00197987	0.00197993	0.00045329	0	0	0.00126263	0.00010193	0.00034728
Snap Pea Pods	0.25714	0.031675	0	0.008313	0.017854	0.002185	0.002539	0	0.025253	0	0	0.00105	0	0.001839
Snow Pea Pods	0.371883	0.026218	0.019538	0.004233	0.015632	0.000882	0.001834	0	0.021516	0	0	0	0	0.001148
Swiss Chard Leaves	0.074886	0.035702	0	0.027169	0.064654	0.003081	0.006897	0	0.018991	0	0	0.001652	0	0.001403
Tomatillo	0.5893998	0.01738077	0.22825826	0.0612546	0.03612464	0.00135257	0.00620496	0.00029178	0.00167988	0.00034476	0.00034556	0.02282085	0	0.00329164
White Button Mushroom Flesh	0.117555	0.016159	0	0.006856	0.001216	0.002341	0.00015	0.00159	0	0	0	0.008738	0	0.002556
White Button Mushroom Skin	0.117555	0.016159	0	0.006856	0.001216	0.002341	0.00015	0.00159	0	0	0	0.008738	0	0.002556
White Onion Peel	0.15805838	0	0.04143889	0.00038118	0.0013241	0.00057056	0.00017848	0	0	0	0	0.0002254	0	0.00036259
Yellow Zucchini Squash	0.242101	0.034165	0	0.011467	0.010869	0.003216	0.0022	0	0.02197	0	0	0.00298	0	0.001506

Table S2.3. (cont.)

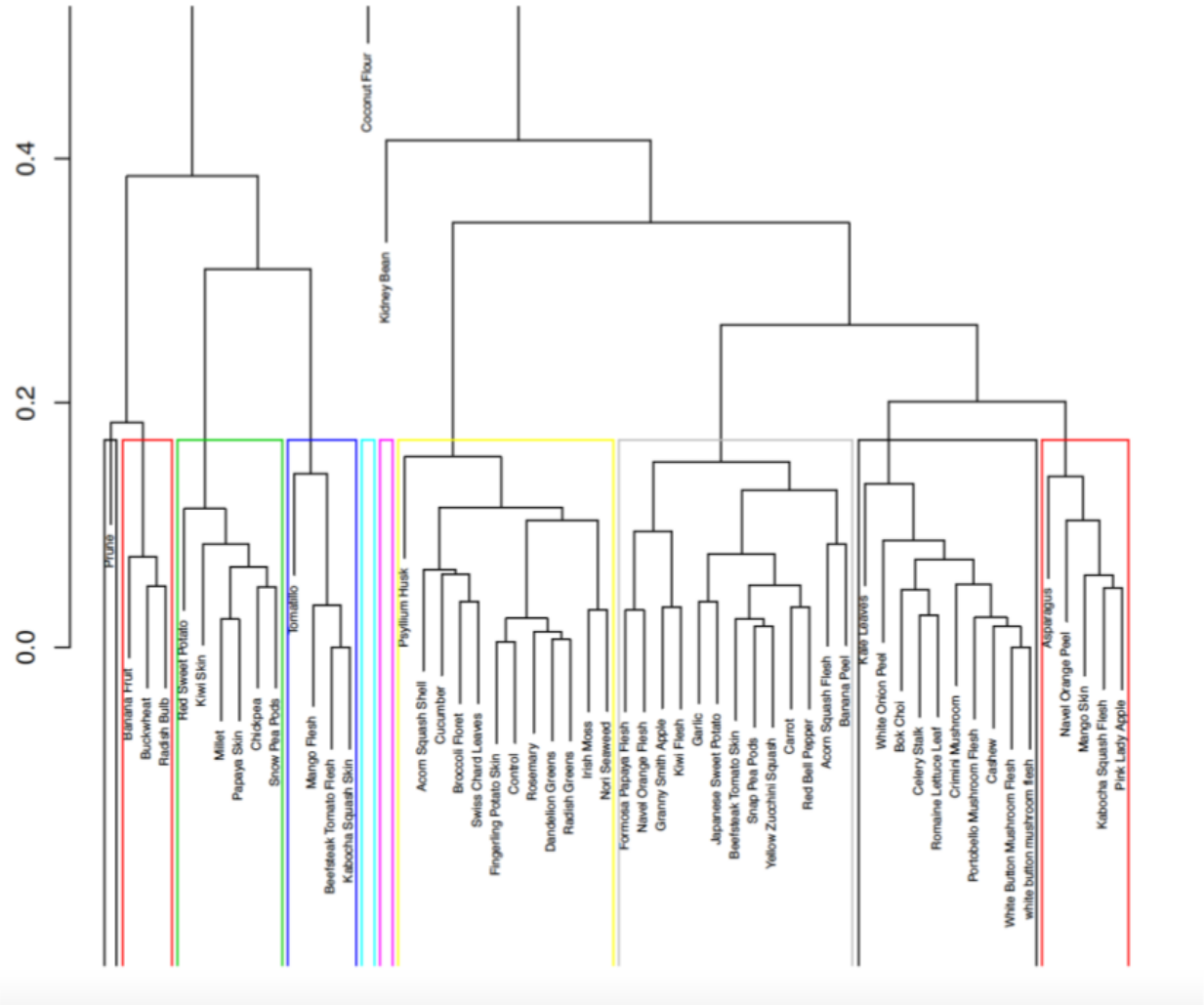

Figure S2.1. Hierarchical clustering analysis of 55 food fibers based on absolute monosaccharide composition. Clustering was performed with DBSCAN and found to exhibit a high degree of noise (31%).

Variable	Day	p-value
Sequencing Run	0	0.001
Sequencing Run	1	0.008
Glucose	1	0.011
Galactose	1	0.021
Fructose	1	0.004
Rhamnose	1	0.005
GalA	1	0.001
GalNac	1	0.002
Mannose	1	0.001
Allose	1	0.037
GlcA	1	0.016
Sequencing Run	2	0.001
Glucose	2	0.008
Galactose	2	0.009
Fructose	2	0.003
Rhamnose	2	0.007
GalA	2	0.001
GalNac	2	0.005
Mannose	2	0.002
Allose	2	0.048

Table S2.4. PERMANOVA of microbiome data from samples taken at 0, 24 and 48 hours of fermentations. PERMANOVA was performed with 999 permutations on a distance matrix of Bray–Curtis distances with the adonis2 function (vegan package). Rarefied 16S rRNA data (rarefaction depth=2509) were used due to >10-fold read differences between samples.